Archives of Environmental Protection
Vol. 50 no. 3 pp. 65–83

PL ISSN 2083-4772
DOI:10.24425/aep.2024.151687

Adsorption of nitrate and phosphate ions using $ZnCl_2$-activated biochars from phytoremediation biomasses

Katlarelo Lenny Sefatlhi[1]*, Venecio U Ultra[1], Majoni Stephen[1], Sylwia Oleszek[2], Trust Manyiwa[1]

[1]Botswana International University of Science and Technology, Department of Earth and Environmental Sciences, Botswana
[2]Kyoto University, Department of Environmental Engineering, Kyoto, Japan.

* Corresponding author's e-mail: sk15000580@studentmail.biust.ac.bw

Keywords: isotherms, surface area, surface morphology, adsorbent, Pyrolysis, adsorbate

Abstract: Mishandling and disposal of post-harvested phytoremediation biomass results in secondary pollution. Biochar production is one of the available technologies for processing post-harvested phytoremediation biomasses. The main objective of this study was to assess the potential adsorption of PO_4^{3-} and NO_3^- ions from a binary solution by $ZnCl_2$-activated phytoremediation biochars. The biochars were activated using $ZnCl_2$ and analyzed for specific surface area, pore size, volume, surface morphology, point of zero charges (pH_{pzc}), surface functional groups, and elemental composition. Subsequently, the adsorption potential for PO_4^{3-} and NO_3^- ions of the activated biochar was investigated. Activation of phytoremediation biochars led to the development of new micropores and increased specific surface area range from 1.62-4.72 $m^2\ g^{-1}$ to 4.75- 55.50 $m^2\ g^{-1}$. $ZnCl_2$ activation reduced the pH_{pzc} values of *Cymbopogon citratus*, *Cymbopogon nardus*, and *Chrysopogon zizanioides* biochars (BCL2, BCC2, and BCV2) from 9.75, 9.50, 9.62 to 5.72, 5.51, and 6.23, respectively. Activated *Chrysopogon zizanioides* biochar (ACBCV2), activated *Cymbopogon nardus* biochar (ACBCC2) and activated *Cymbopogon citratus* biochar (ACBCL2) showed maximum potential phosphate ion adsorption capacities of 115.70, 101.74, and 270.59 mg g^{-1}, respectively. ACBCL2, ACBCC2, and ACBCV2 indicated maximum potential nitrate ion adsorption capacities of 155.78, 99.42, and 117.71 mg g^{-1}. BCC2, BCL2, ACBCV1, ACBCV2, and ACBCC2 best fitted the Langmuir linear form 1 model during NO_3^- adsorption. The results obtained in this study showed that ZnCl2-activated phytoremediation biochars have the potential to remove PO_4^{3-} and NO_3^- ions from PO_4^{3-} and NO_3^- ions binary solution.

Introduction

In recent decades, phytoremediation technology has been employed to rehabilitate contaminated lands. This technology involves selecting and utilizing particular plants or vegetation to extract and translocate pollutants from the soil to plant tissues for post-harvest (He et al. 2020). To date, the disposal of heavy-metal-contaminated biomass from phyto-remediated environments remains a global issue. Improper handling of phytoremediation biomass can easily lead to secondary pollution (Ghosh and Singh 2005). In this study, phytoremediation biomass refers to biomass harvested from heavy metal-rich BCL Cu-Ni mine tailings, while non-phytoremediation biomass refers to biomass grown in non-heavy metal-contaminated soil. One of the major drawbacks of industrialization is environmental pollution. The quest for enhanced food production has led to increased applications of fertilizers in the agricultural sector. The leaching of phosphorous and nitrogen compounds from agricultural fields into aquatic systems results in their enrichment, leading to eutrophication (Wang et al. 2015, Yao et. 2012).

Due to the environmental problems caused by by high concentrations of PO_4^{3-} and NO_3^- ions, it is crucial to treat wastewater containing nitrates and phosphates before discharging it into the environment. One effective method for purifying wastewater is adsorption, in which carbon-based materials are the adsorbents of choice. While biomass-derived activated carbon and biochar have received considerable attention as adsorbents, the use of phytoremediation biomass as a precursor material has not been adequately explored. Biochar is a fine-grained, carbon-rich biomaterial produced by the slow pyrolysis of biomass (Yağmur and Kaya 2021). Its special properties, such as a porous structure and high carbon content, broaden its application prospects in both environmental and agricultural sectors (Xie et al. 2015). Biochar activation is the process of increasing the adsorption sites or capacity of biochar through physical or chemical mechanisms (Gámiz et al. 2019). Physical activation involves ball milling and

grinding of biochar (Pena et al. 2020), gaseous modification by steam, carbon dioxide, air, or ozone, and thermal modification by conventional heating and microwave irradiation. Chemical activation involves treating biochar with oxidizers, acids, or bases (Williams and Reed 2004).

The main aim of biochar activation is to induce reactive functional groups on biochars, enhance the specific surface area, develop porous structure, and alter the surface charge of biochars to improve the affinity between biochar and adsorbates (Borchard et al. 2012, Deng et al. 2021). According to a study by Paredes et al. (2021), various adsorbents can be modified using different activators such as KOH, NaOH, H_3PO_4, and $ZnCl_2$. $ZnCl_2$ is particularly preferred for the activation of carbon-based materials such as biochars since it enhances pore development, increases the specific surface area of the carbonaceous structure, and typically results in a high yield of modified carbon (Menya et al. 2018). The low melting point of $ZnCl_2$ (283-293 °C) enables it to easily contact the carbon surface at activation temperatures above 500 °C (Li et al. 2020). Ideally, $ZnCl_2$ activation should be performed at temperatures above 500 °C taking into consideration the lignocellulosic composition of the feedstock. However, performing $ZnCl_2$ activation at higher temperatures (above 600 °C) can result in lower biochar yield (Bouchemal et al. 2009, Hock and Zaini 2018). To maximize biochar production for adsorption studies, the procedures by Abd et al. (2019) and Huang et al. (2024) were adopted.

Adsorption technology results in a high accumulation of contaminants on the surface of adsorbent, decreasing their concentrations in treated wastewater (Wu et al. 2019). Contaminant adsorption in wastewater can be achieved by either chemical or physical means. Physical adsorption involves the adsorbate deposition on the surface of the adsorbent without the forming chemical bonds (Inyang et al. 2016), whereas chemical adsorption involves chemical complexation between the adsorbent and contaminants (Xia et al. 2019). The mechanisms for removing PO_4^{3-} and NO_3^- ions by adsorption generally include hydrogen bonding, ion exchange, co-precipitation, complexation, and electrostatic adsorption (Gizaw et al. 2021, Barquilha and Braga 2021).

The objectives of this study were to: (1) determine the influence of $ZnCl_2$ activation on the specific surface area, pore size, and volume, point of zero charges, and surface morphology of phytoremediation biochars, and (2) evaluate the potential of activated biochar as adsorbent(s) for PO_4^{3-} and NO_3^- ions from a binary solution. Several studies have investigated the removal of PO_4^{3-} and NO_3^- ions from wastewater using $ZnCl_2$-activated biochar from different feedstocks (Thue et al. 2022, Biswas et al. 2023, Lie et al. 2018). However, this is the first study to (1) assess the effect of $ZnCl_2$ activation on the physicochemical properties of biochar derived from phytoremediation biomass, and (2) determine the potential of $ZnCl_2$-activated biochar from phytoremediation biomass as adsorbents for PO_4^{3-} and NO_3^- ions from a binary solution.

Materials and methods

Biomass and Biochar production

Phytoremediation and non-phytoremediation biomasses were produced by growing *Cymbopogon citratus*, *Cymbopogon nardus,* and *Chrysopogon zizanioides* grasses in Bamangwato Concessions Limited (BCL) Cu-Ni mine tailings and uncontaminated soil. Biochars were produced by pyrolyzing these biomasses at 550°C in an inert environment for 30 minutes, and the chemical characteristics of the resulting biochar were analyzed. According to Ultra et al. (2022), the BCL mine tailings are highly acidic, with a pH value of 2, and contain heavy metal concentrations of 154.31, 220.27, 1137.53, 552.81, 2025.22, and 5311.62 mg kg^{-1} for As, Zn, Mn, Pb, Ni, and Cu, respectively. *Cymbopogon citratus*, *Cymbopogon nardus,* and *Chrysopogon zizanioides* grass species were used in this study for the phytoremediation of the BCL Cu-Ni mine tailings.

Activation of phytoremediation and non-phytoremediation biochars

Chemical activation of phytoremediation and non-phytoremediation biochars was carried out using 0.1 M $ZnCl_2$ (99% purity grade). Biochar and $ZnCl_2$ solution were mixed in a ratio of 10g:100 mL. The mixing was performed at 25°C for 24 hours. After mixing, the slurry was dried in an oven at 105°C overnight. The modified biochar was then washed with 0.1 M hydrochloric acid (HCl, 36% purity grade) by stirring for 4 hours at room temperature. The activated biochar was then washed several times with deionized water. The resultant biochar was dried at 110°C for 24 hours (Abd et al. 2019).

Physicochemical characterization of non-activated (ordinary) and activated biochars

The specific surface area was determined following the multipoint Brunaer-Emmett-Teller (BET) method in a relative pressure range of 0.05 to 0.3 using a BELSORP-MINI II BET surface area and pore size analyzer (Lee and Park 2013). The t-method was used to estimate micropore volume and external surface area (Lawal et al. 2021, Buentello et al. 2020). The monolayer thickness was computed using the following equation (eq 1) for carbon-like materials:

$$t = 2.98 + 6.45\left(\frac{p}{p^0}\right) + 0.88\left(\frac{p}{p^0}\right)^2 \qquad \text{(eq 1)}$$

where *t* refers to the monolayer thickness and p/p^o is the relative pressure of nitrogen.

The micropore surface area was calculated by subtracting the external surface area from the specific surface area obtained using the BET method. The volume of the mesopore was obtained by subtracting the micropore volume from the total pore volume. Assuming that all pores are cylindrical, straight, and not interconnected, the average pore size was estimated using the following formula:

$$d_{\text{average}} = \frac{4\text{Vt}}{\text{SSA}} \qquad \text{(eq 2)}$$

where $d_{average}$ is the average pore size, V_t is the total pore volume, and SSA is the specific surface area (Hung et al. 2017, Muzyka et al. 2023). The surface morphology of ordinary and activated biochar samples was characterized using JEOL JSM-7100F Field Emission Scanning Electron Microscope at a working distance, voltage, and magnification of 10 mm, 15.0 kV, and x850 µm, respectively. Before surface morphology analysis, biochar samples were first coated with carbon.

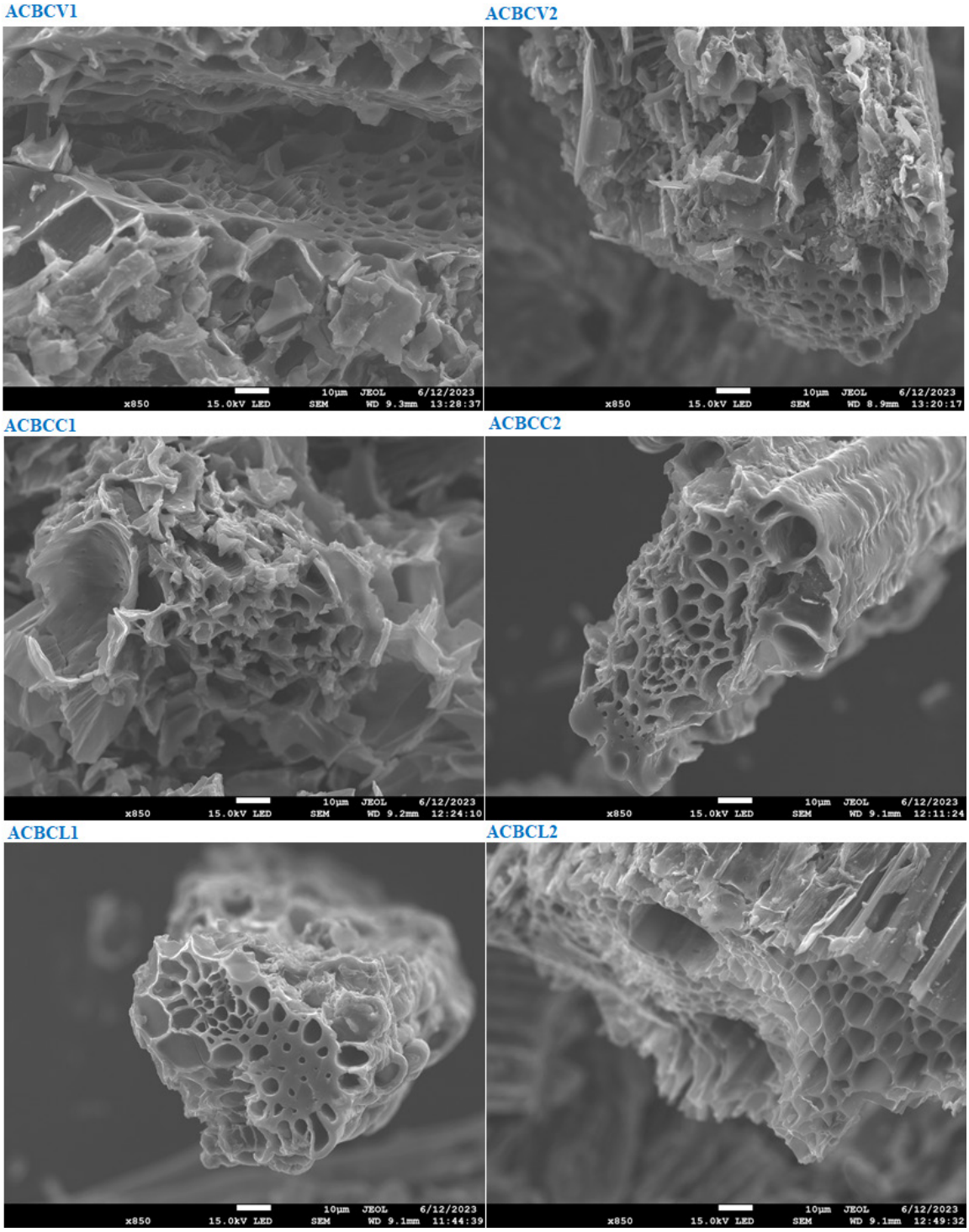

Figure 1. Surface morphologies activated biochars derived from phytoremediation and non-phytoremediation biomasses.
ACBCV1: activated *Chrysopogon zizanioides* non-phytoremediation biochar, ACBCV2: activated *Chrysopogon zizanioides* phytoremediation biochar, ACBCC1: activated *Cymbopogon nardus* non-phytoremediation biochar, ACBCC2: activated *Cymbopogon nardus* phytoremediation biochar, ACBCL1: activated *Cymbopogon citratus* non-phytoremediation biochar, ACBCL2: activated *Cymbopogon citratus* phytoremediation biochar.

The point of zero charge of biochar samples was determined using a modified procedure from the study conducted by Liu et al. (2015). The pH of a 0.01 M NaCl (99% purity grade) solution was adjusted to 2, 4, 6, 8, 10, and 12 using either 0.1 M HCl (36% purity grade) or 0.1 M NaOH (99% purity grade) solutions. At a selected pH, 20 ml of the 0.01 M NaCl solution was mixed with 0.2 g of biochar and oscillated for 48 h. The change in pH (pH_f - pH_i) was plotted against the initial pH, and the points of zero charge were determined from where the graphs intercepted the x-axis. Mineralogical, surface functional group, and elemental analyses of activated biochars were conducted using a Bruker D8 Advance powder diffractometer (using a Cu Kα radiation source), a Fourier Transformer Infrared Spectrometer (USA Nicolet IS5), and an X-ray Fluorescence (XRF) spectrometer emitting 3 beams (beam 1 at a voltage of 50 kV, beam 2 at a voltage of 40 kV, and beam 3 at a voltage of 10 kV) using soil mode, with each beam running for 30 seconds.

PO_4^{3-} and NO_3^- ions batch adsorption tests

A binary solution of phosphate and nitrate ions was prepared by dissolving sodium nitrate ($NaNO_3$) and potassium dihydrogen phosphate (KH_2PO_4) salts in deionized water with a resistivity value of 5.10 MΩcm following the procedure described by Alagha et al. (2020). Batch adsorption tests for PO_4^{3-} and NO_3^- ions were conducted under varying conditions: (a) biochar dosages, (b) solution pH values, (c) contact times, and (d) initial ion concentrations. The effect of biochar dosage (0, 20, 100, 200, 1000, and 2000 mg/L) was examined in 40 ml of PO_4^{3-} and NO_3^- ions binary solution (50 mg L^{-1}) for 24 h at an orbital speed of 180 r.p.m.

The effect of solution pH (2, 4, 6, 8, 10, and 12) was investigated using a selected biochar dosage (0.04 g) in 40 ml of solution containing PO_4^{3-} and NO_3^- ions (50 mg/L) at an orbital speed of 180 rpm for 24 h. The pH was adjusted using either 0.1 M HCl or 0.1 M NaOH. The effect of contact time (0.3, 0.5, 1, 2, 4, and 8 h) was evaluated with the same biochar dosage (0.04 g) in 40 ml of a binary solution of PO_4^{3-} and NO_3^- ions (50 mg/L) at a solution pH of 6 and an orbital speed of 180 rpm for 24 hr. The influence of the initial concentration of PO_4^{3-} and NO_3^- ions (20, 50, 100, 200, 300 to 500 mg L^{-1}) was analyzed by adding the selected biochar dosage (0.04 g) into 40 ml of PO_4^{3-} and NO_3^- solution and shaking it at an orbital speed of 180 rpm for 1h at a solution pH of 6.

Analysis of PO_4^{3-} and NO_3^- ion concentrations

After the adsorption experiments, all mixtures were filtered using a 0.45 µm nylon syringe filter, and the concentrations of PO_4^{3-} and NO_3^- ions were analyzed using a Thermo Fisher DS 120 Ion Chromatography system.

Computation of adsorption capacities

The adsorption capacity values were computed using the following equations (Mehdizadeh et al. 2014):

$$Q_e = \frac{(C_i - C_e)V}{M} \quad \text{(eq 3)}$$

where Q_e is equilibrium adsorption capacity (mg g^{-1}), C_i - initial concentration (mg L^{-1}), C_e - equilibrium concentration

Table 1. Equilibrium adsorption isotherm models used in this study

Isotherm model	Linear Form	Plot	Parameter	Eq.no
	Form 1			
Langmuir $q_e = \frac{q_m K_L C_e}{1 + K_L C_e}$	$\frac{1}{q_e} = \left(\frac{1}{K_L q_m}\right)\frac{1}{C_e} + \frac{1}{q_m}$ Form 2	$\frac{1}{q_e}$ vs $\frac{1}{C_e}$	q_e: equilibrium adsorption capacity (mg g^{-1}) q_m: maximum adsorption capacity of the adsorbent (mg g^{-1}) K_L: Langmuir adsorption constant (L mg^{-1}) C_e: equilibrium concentration (mg L^{-1})	(4)
	$\frac{1}{C_e} = -K_L + q_m K_L \frac{1}{q_e}$ Form 3	$\frac{1}{C_e}$ vs $\frac{1}{q_e}$		(5)
	$\frac{1}{qe} = q_m - \frac{1}{K_L}\frac{q_e}{C_e}$	q_e vs $\frac{q_e}{C_e}$		(6)
	Form 4			
	$\frac{q_e}{C_e} = K_L q_m - K_L q_e$	$\frac{q_e}{C_e}$ vs q_e		(7)
Freundlich $q_e = K_F C_e^{\frac{1}{n}}$	$\log(q_e) = \log K_F + \frac{1}{n}\log C_e$	$\log q_e$ vs $\log C_e$	K_F: maximum adsorption capacity (mg g^{-1}) n: adsorption strength	(8)
Temkin $q_e = \frac{RT}{b_T \ln A_T C_e}$	$q_e = \frac{RT}{b_T \ln A_T} + \left(\frac{RT}{b_T}\right)\ln C_e$	q_e vs $\ln C_e$	R: gas constant (Jmol^{-1} K^{-1}) T: absolute temperature (K) b_T: Constant related to the heat of adsorption (J mol^{-1}) A_T: Temkin isotherm equilibrium binding constant (L mg^{-1})	(9)
Dubinin Raduskevich $q_e = (q_s)\exp(-B_D\epsilon^2)$	$\ln(q_e) = \ln(q_s) - B_D\epsilon^2)$	$\ln(q_e)$ vs ϵ^2	q_m: maximum adsorption capacity of the adsorbent B_D: constant of adsorption energy (mol^2 kJ^{-2}) ϵ: energy of adsorption	(10)

Note: Eq.no refers to equation number.

(mg L^{-1}), V - volume of the solution (L), M - mass of the adsorbate (g).

Adsorption isotherms used in this study

To determine the applicable equilibrium adsorption isotherm, the equilibrium adsorption data were fitted to 4 isotherm models: the Langmuir model, the Freundlich model, the Temkin model, and the Dubinin-Radushkevish model (Foo and Hameed 2010, Itodo et al. 2010). The models are shown in Table 1. The adsorption isotherm constants were computed from the slopes and intercepts of the linear equations. The best fitting isotherm for PO_4^{3-} and NO_3^- ions adsorption data was chosen based on the regression coefficient closest to 1.

The separation factors were calculated and plotted for biochars that best fitted the Langmuir adsorption isotherm. The separation factor R_L was calculated using equation 11:

$$R_L = \frac{1}{1+K_L C_i} \quad \text{(eq 11)}$$

where R_L is the dimensionless separation factor, K_L is the Langmuir constant (L mg^{-1}), and C_i is the initial concentration of the adsorbate (mg L^{-1}). The separation factor indicates the favorability of adsorption: for $R_L>1$, $R_L=1$, $0<R_L<1$, and $R_L = 0$ the adsorption is unfavorable, linear, favorable, and irreversible, respectively (Foo and Hameed 2010).

Experimental quality assurance and statistical analysis

The point of zero charge (PZC) and adsorption experiments were replicated 3 times to enhance the precision of the experimental results. The PZC data were subjected to analysis of variance (ANOVA) to assess significant differences between 2 factors (grass types and biomass sources). Turkey's homogeneity test was used to determine whether there was a significant difference when the mean comparison was made at a 0.05 probability level.

Results and Discussion

Physicochemical characterization of non-activated (ordinary) and activated biochars

Table 2 presents the results of specific surface area, total pore volume, and average pore diameter for all biochars. Ordinary biochars derived from phytoremediation biomasses (BCV2, BCC2, and BCL2) exhibited higher specific surface areas compared to non-phytoremediation biochars. $ZnCl_2$ activation increased the specific surface areas of BCV2, BCC2, and BCL2 from 1.61 to 5.61 m^2 g^{-1}, 4.51 to 5.23 m^2 g^{-1}, and 4.75 to 50.50 m^2 g^{-1}, respectively. Similar results have been reported by Yan et al, who observed that $ZnCl_2$ activation increased the specific surface area of biochar derived from aerobic granular sludge from 6.34 m^2 g^{-1} to 852.41 m^2 g^{-1} (Yan et al. 2020). In this study, the total pore volume of non-phytoremediation biochars increased from a range of 0.36- 0.46 cm^3 g^{-1} to 0.44-13.00 cm^3 g^{-1} after $ZnCl_2$ modification. For phytoremediation biochars, the total pore volume increased from a range of 8.23-10.05 cm^3 g^{-1} to 13.35-71.84 cm^3 g^{-1} (62.21-614.83%). Activated *Cymbopogon citratus* phytoremediation biochar (ACBCL2) showed higher micropore and mesopore volumes, corresponding to 2.34 cm^3 g^{-1} and 69.49 cm^3 g^{-1}, respectively.

Table 2. Specific surface area, total pore volume, and average pore diameter of ordinary and activated phytoremediation and non-phytoremediation biochars

Sample code	Specific surface area (m^2/g)	External surface area (m^2/g)	Micropore surface area (m^2/g)	Total pore volume (cm^3/g)	Micropore volume (cm^3/g)	Mesopore volume (cm^3/g)	Average pore size (nm)
BCV1	1.43	-	-	0.36	0.50	0.14	0.04
BCV2	1.61	0.08	1.53	8.23	0.36	7.87	0.08
BCC1	1.38	-	-	0.46	0.35	0.11	0.12
BCC2	4.51	0.19	4.32	8.65	0.39	8.26	0.02
BCL1	1.50	0.45	4.30	0.38	-	-	0.04
BCL2	4.75	0.12	1.38	10.05	0.34	9.71	0.03
ACBCV1	4.57	0.29	4.28	13.00	-	-	0.01
ACBCV2	5.61	0.37	5.24	13.35	-	-	0.07
ACBCC1	3.12	0.15	2.97	1.02	0.21	0.81	0.13
ACBCC2	5.23	0.31	4.92	17.55	0.98	16.57	0.01
ACBCL1	15.12	3.06	14.11	0.44	-	-	0.01
ACBCL2	55.50	1.01	52.44	71.84	2.34	69.49	0.01

Note: BCV1: *Chrysopogon zizanioides* non-phytoremediation biochar, BCV2: *Chrysopogon zizanioides* phytoremediation biochar,
BCC1: *Cymbopogon nardus* non-phytoremediation biochar, BCC2: *Cymbopogon nardus* phytoremediation biochar,
BCL1: *Cymbopogon citratus* non-phytoremediation biochar, BCL2: *Cymbopogon citratus* phytoremediation biochar,
ACBCV1: activated *Chrysopogon zizanioides* non-phytoremediation biochar, ACBCV2: activated *Chrysopogon zizanioides* phytoremediation biochar,
ACBCC1: activated *Cymbopogon nardus* non-phytoremediation biochar, ACBCC2: activated *Cymbopogon nardus* phytoremediation biochar,
ACBCL1: activated *Cymbopogon citratus* non-phytoremediation biochar, ACBCL2: activated *Cymbopogon citratus* phytoremediation biochar.

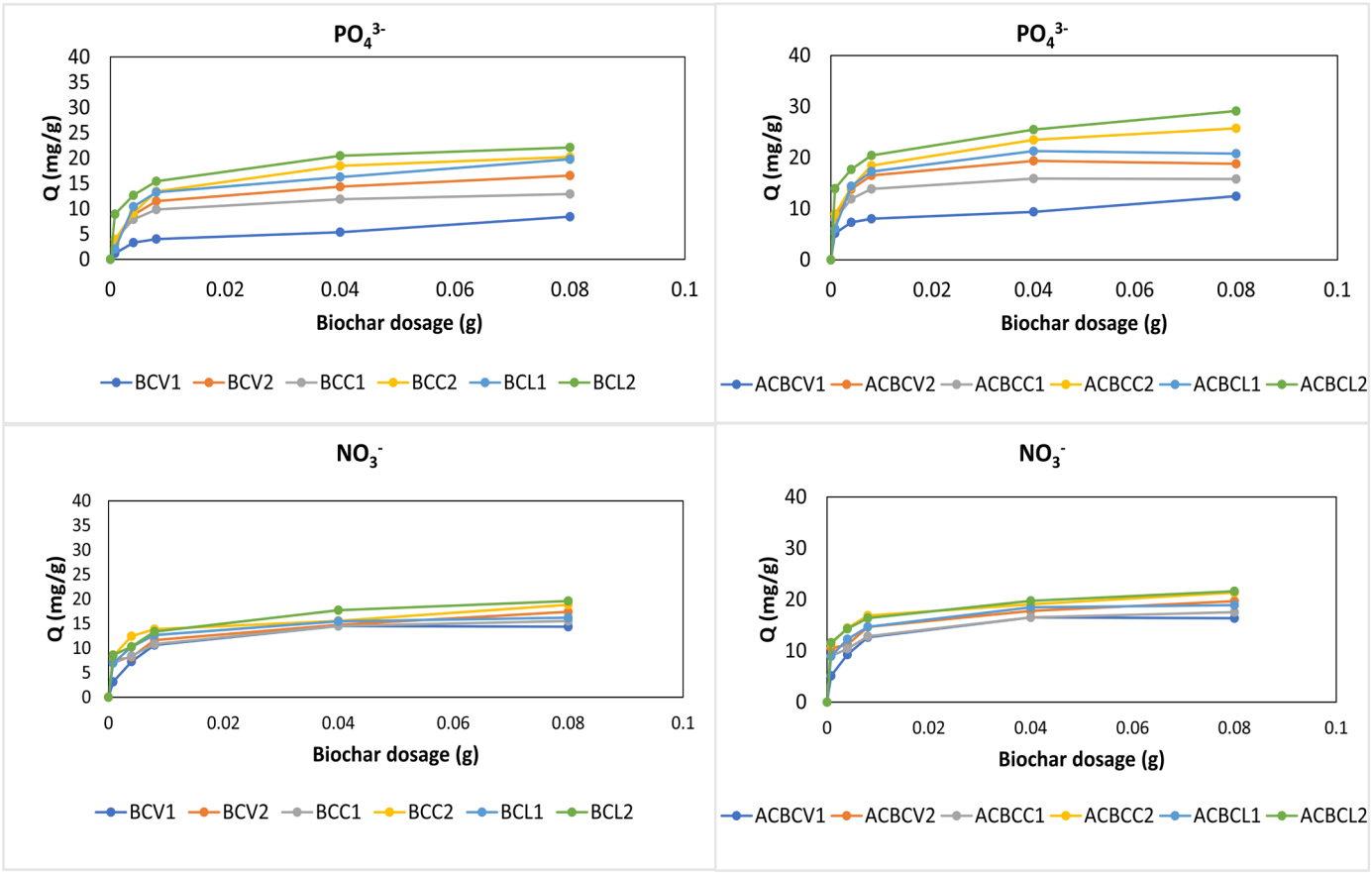

Figure 2. Effect of biochar dosage on PO_4^{3-} and NO_3^- adsorption **by ordinary and activated biochars derived from phytoremediation biomasses**. Q: adsorption capacity,
BCV1: *Chrysopogon zizanioides* non-phytoremediation biochar, BCV2: *Chrysopogon zizanioides* phytoremediation biochar,
BCC1: *Cymbopogon nardus* non-phytoremediation biochar, BCC2: *Cymbopogon nardus* phytoremediation biochar,
BCL1: *Cymbopogon citratus* non-phytoremediation biochar, BCL2: *Cymbopogon citratus* phytoremediation biochar,
ACBCV1: activated *Chrysopogon zizanioides* non-phytoremediation biochar, ACBCV2: activated *Chrysopogon zizanioides* phytoremediation biochar,
ACBCC1: activated *Cymbopogon nardus* non-phytoremediation biochar, ACBCC2: activated *Cymbopogon nardus* phytoremediation biochar,
ACBCL1: activated *Cymbopogon citratus* non-phytoremediation biochar, ACBCL2: activated *Cymbopogon citratus* phytoremediation biochar.

Variations in specific surface areas among ordinary biochar derived from different grass types could be attributed to differences in their cellular contents. Lee and Shin (Lee and Shin 2021) associated a small biochar surface area with high lignin content, which does not easily decompose at low temperatures. Du et al. attributed the higher specific surface area of phytoremediation biochars to the potential catalytic effect of heavy metals in the decomposition and dehydration of organic material (Du et al. (2019). Our earlier work (Sefatlhi et al. 2023) showed that phytoremediation biochars exhibited higher heavy metal contents. Table S1 also indicates that activated phytoremediation biochars had higher heavy metal contents compared to non-phytoremediation biochars. ACBCL2 had higher concentrations of Al, Ni, Cu, As, and Zn, while ACBCV2 exhibited a higher concentration of Rb, as shown in Table S1.

Similarly, Liu et al. (2014) found out that pyrolysis of biomass loaded with Cu and Fe leads to the generation of biochar with a higher surface area due to the participation of Cu and Fe in the formation of a micro-porous structure during pyrolysis. The comparatively higher heavy metal content in phytoremediation biomass may have a similar effect on the formation of a porous structure, as reported by Liu et al. (2014) for Fe and Cu. Activation of biochar with $ZnCl_2$ has been shown to decompose cellulosic material, which is beneficial for the generation of micropores and results in a higher surface area (Zhao et al. 2017, Angin et al. 2013).

The average pore diameters of both ordinary and activated biochars derived from phytoremediation and non-phytoremediation biomasses were below 2 nanometers (nm), which are classified as micropores according to the International Union of Pure and Applied Chemistry (IUPAC) system (Gray et al. 2014). The average pore diameters of activated phytoremediation biochars were slightly lower than those of activated non-phytoremediation biochars, except for ACBCV2. $ZnCl_2$ activation slightly reduced the average pore diameter of all biochars, except for BCC1. A similar effect was observed in a study by Guo et al. (2019) who found decreased average pore diameter (from 3.533 to 2.241 nm) in $ZnCl_2$-activated biochar produced from rice husk (Guo et al. 2019).

Figure S1 illustrates the surface functional group profile of activated biochars derived from phytoremediation and non-phytoremediation biomasses. Principal component analysis, shown in Figure S2, revealed that the composition of alcohols, allenes, thiocyanates, carboxylic acids, alkenes, alkynes, and alkanes increased from ACBCC1 and ACBCL1 to ACBCC2

and ACBCL2. XRD analysis (Figure S3) indicated that the intensities of quartz and sphalerite peaks were higher in ACBCC2 compared to the corresponding activated non-phytoremediation biochars. The higher intensity of the mineral peaks in phytoremediation biochar suggests enhanced crystalline properties, possibly due to enriched heavy metalloids (He et al. 2019).

Figure 2 shows that activated phytoremediation biochars exhibit a more porous structure compared to activated non-phytoremediation biochars. Among them, ACBCL2 displayed a more pronounced porous structure than ACBCC2 and ACBCV2. The $ZnCl_2$ activation process results in the widening of the existing pores and the development of new ones, which increases the specific surface area and pore volume of the biochar (Angın et al. 2013). The $ZnCl_2$ activation enhances intercellular- and intracellular spaces by breaking the bonds in cellulose molecules, leading to increased surface porosity (Machado et al. 2020). The high porosity observed in activated phytoremediation biochars may be attributed to the catalytic effect of the impregnated heavy metals, which facilitate the decomposition and dehydration of organic material (Du et al. 2019).

The solution pH of the PO_4^{3-} and NO_3^- ions binary mixture was lower than all the pHpzc values of both phytoremediation and non-phytoremediation biochars, indicating that biochar samples carried net positive charges at the solution pH. The pH_{pzc} values of ordinary biochars decreasing in the following order: 11.76>9.75>9.73>9.63>9.50 corresponding to BCV1, BCV2, BCL1, BCC1, BCL1, and BCC2, respectively. For non-phytoremediation biochars, BCV1 had the highest pH_{pzc} value (11.76), followed by BCL1 (9.73) and BCC1 (9.72). $ZnCl_2$ activation reduced the pH_{pzc} values of BCV2, BCC2, and BCL2 from 9.75, 9.50, and 9.62 to 5.72, 5.51, and 6.23, respectively. Table 3 indicates that activated phytoremediation biochars had lower pHpzc values compared to activated non-phytoremediation biochars. According to Zhao et al. (2015), the net surface charge of biochar is affected by organic functional groups and present minerals. The study further attributes low pH_{pzc} values to the presence of inorganic constituents such as heavy metals. Table S1 supports that activated phytoremediation biochars had higher heavy metal contents compared to activated non-phytoremediation biochars. The point of zero charge values in the acidic region after activation of biochar using $ZnCl_2$ indicates the predominance of acidic functional groups (Thue et al. 2022, Zubir and Zaini 2020).

PO_4^{3-} and NO_3^- ions batch adsorption tests

Increasing biochar dosage led to increased adsorption of PO_4^{3-} and NO_3^- ions by both ordinary and activated biochars with most of biochar samples reaching their optimum adsorption point at a dosage of 0.04 g (Figure 3). Beyond 0.04 g, the increase in adsorption was minimal, so this value was adopted as the lowest dosage for further studies. The adsorption capacities of PO_4^{3-} and NO_3^- ions were higher in biochars derived from phytoremediation biomasses (Figure 3). The PO_4^{3-} ion adsorption capacities decreased in the following order: 22.13>20.24>16.57 mg g^{-1}, corresponding to BCL2, BCC2, and BCV2, respectively, at a biochar dosage of 0.08 g. $ZnCl_2$ activation enhanced the PO_4^{3-} adsorption capacities of BCL2, BCC2, and BCV2 by 7.01(13.47%), 2.12 (27.81%), and 5.06 (31.78%) mg g^{-1}, respectively. Similarly, Ahmed et al. (2016) reported that nitrate and phosphate ions in wastewater were better adsorbed by $ZnCl_2$-activated biochars compared to ordinary biochars. The NO_3^- ions adsorption capacities of activated phytoremediation biochars increased in the

Table 3. Point of zero charges of ordinary and activated non-phytoremediation and phytoremediation biochars

Ordinary biochars		Activated biochars	
Sample name	pHpzc	Sample name	pHpzc
BCV1	11.76a	ACBCV1	6.38b
BCV2	9.75b	ACBCV2	5.72b
BCC1	9.72b	ACBCC1	7.08a
BCC2	9.50d	ACBCC2	5.51c
BCL1	9.73b	ACBCL1	6.29b
BCL2	9.62c	ACBCL2	6.23b
PO43- & NO3- solution	5.34		
TG	0.000***		0.002***
SB	0.036**		0.001***
TG*SB	ns		ns

Note: Pzc refers to point of zero charges,

BCV1 = *Chrysopogon zizanioides* non-phytoremediation biochar, BCV2 = *Chrysopogon zizanioides* phytoremediation biochar,
BCC1 = *Cymbopogon nardus* non-phytoremediation biochar, BCC2 = *Cymbopogon nardus* phytoremediation biochar,
BCL1 = *Cymbopogon citratus* non-phytoremediation biochar, BCL2 = *Cymbopogon citratus* phytoremediation biochar,
ACBCV1: activated *Chrysopogon zizanioides* non-phytoremediation biochar, ACBCV2: activated Chrysopogon zizanioides phytoremediation biochar,
ACBCC1: activated Cymbopogon nardus non-phytoremediation biochar, ACBCC2: activated Cymbopogon nardus phytoremediation biochar,
ACBCL1: activated Cymbopogon citratus non-phytoremediation biochar, ACBCL2: activated Cymbopogon citratus phytoremediation biochar
TG = type of grass, SB = biomass source.

[1]Means within the same column, followed by the same letter(s) are not significantly different according to Turkey's homogeneity test at 5% significance.
* = significant, ** = highly significant, *** = very highly significant; ns = non-significant.

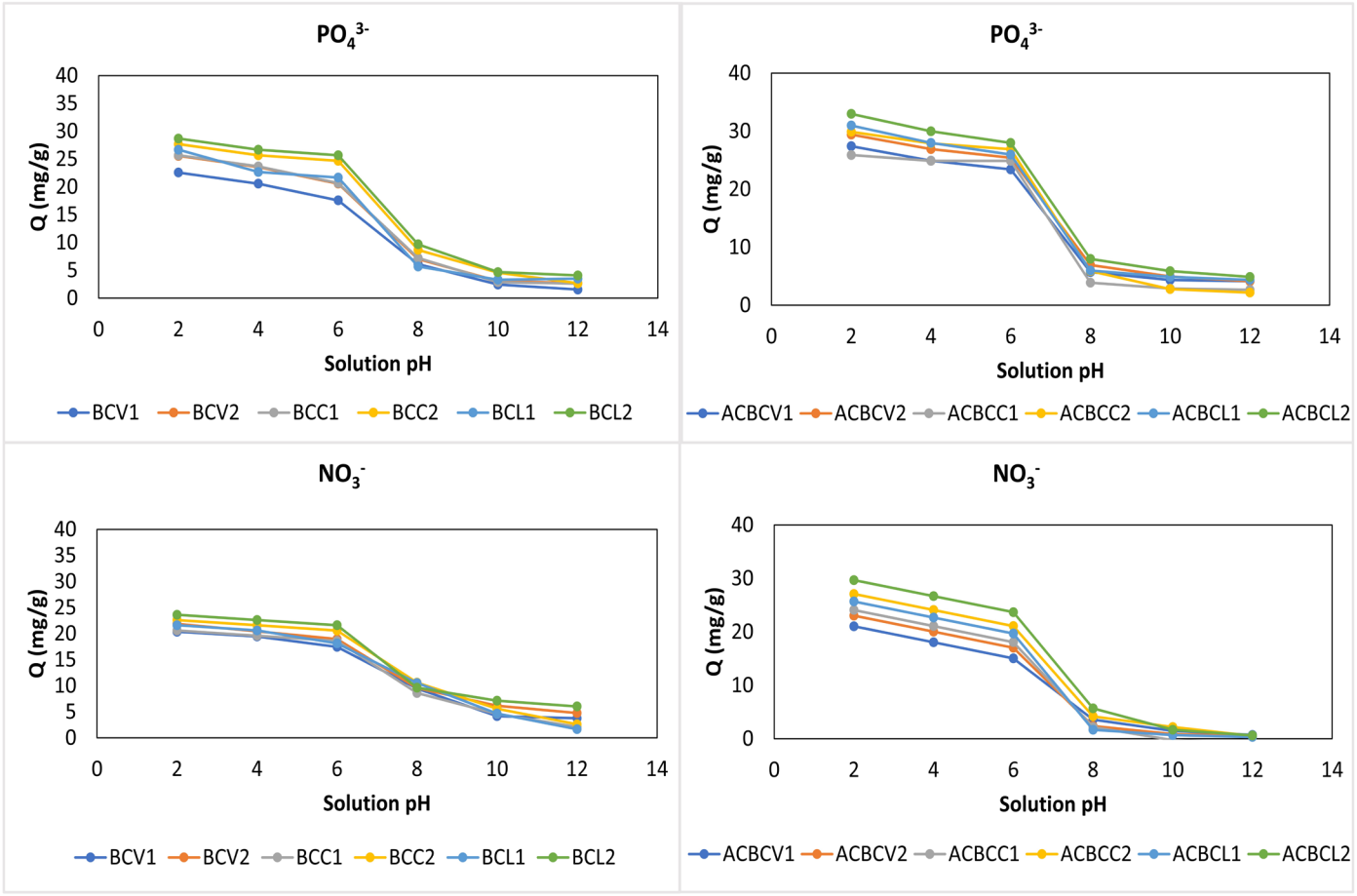

Figure 3. Effect of solution pH on PO_4^{3-} and NO_3^- adsorption **by ordinary and activated biochars derived from phytoremediation biomasses.** Q: adsorption capacity,
BCV1: *Chrysopogon zizanioides* non-phytoremediation biochar, BCV2: *Chrysopogon zizanioides* phytoremediation biochar,
BCC1: *Cymbopogon nardus* non-phytoremediation biochar, BCC2: *Cymbopogon nardus* phytoremediation biochar,
BCL1: *Cymbopogon citratus* non-phytoremediation biochar, BCL2: *Cymbopogon citratus* phytoremediation biochar,
ACBCV1: activated *Chrysopogon zizanioides* non-phytoremediation biochar, ACBCV2: activated *Chrysopogon zizanioides* phytoremediation biochar,
ACBCC1: activated *Cymbopogon nardus* non-phytoremediation biochar, ACBCC2: activated *Cymbopogon nardus* phytoremediation biochar,
ACBCL1: activated *Cymbopogon citratus* non-phytoremediation biochar, ACBCL2: activated *Cymbopogon citratus* phytoremediation biochar.

following order: 17.39<18.85<19.61 mg g^{-1}, corresponding to BCV2, BCC2, and BCL2, respectively. The NO_3^- ion adsorption capacities of ACBCL2, ACBCC2, and ACBCV2 were higher than those of the corresponding ordinary biochars by 2.97 (10.26%), 2.50 (13.26%), and 2.28 (13.17%) mg g^{-1}, respectively, at a biochar dosage of 0.08 g. PO_4^{3-} ions were adsorbed more effectively than NO_3^- ions by both ordinary and activated biochars .

Wang et al. explicated that increasing biochar dosage enhances the reactive functional groups and the contact area for the adsorbate adsorption (Wang et al. 2021). The complex mechanisms of adsorbate adsorption onto the surface of the adsorbent primarily involve ligand exchange, precipitation, hydrogen bonding, surface complexation, ion exchange, electrostatic attraction, and weak van der Waals forces (Priya et al. 2022). Phytoremediation and non-phytoremediation biochars used in this study were protonated at solution pH values lower than their pH_{pzc} values, enabling electrostatic attraction of PO_4^{3-} and NO_3^- ions onto biochar surfaces. The electrostatic attraction process entails the deposition of oppositely charged adsorbates onto a biochar matrix (Feng et al. 2022). This electrostatic attraction process is affected by the solution pH.

Equations 12 and 13 illustrate the electrostatic attraction of $PO_4^{3-}/HPO_4^{2-}/H_2PO_4^-/NO_3^-$ onto the positively charged phytoremediation and non-phytoremediation biochars:

$$M^{n+} + PO_4^{3-}/HPO_4^{2-}/H_2PO_4^- \longrightarrow M^{n+} \ldots PO_4^{3-}/HPO_4^{2-}/H_2PO_4^- \quad \text{(eq 12)}$$

$$M^{n+} + NO_3^- \longrightarrow M^{n+} \ldots NO_3^- \quad \text{(eq 13)}$$

$M^{n+}$is positive charge on biochar surface.

According to Zhang et al. (2020), the primary adsorption mechanism of PO_4^{3-} ions from wastewater is mainly due to the formation of calcium and magnesium phosphates. Yang et al. described the precipitation reactions of phosphorus oxyanions with Ca^{2+} and Mg^{2+} on biochar (Yang et al. 2021), as indicated in equations (eq)14, 15, 16, and 17:

$$Mg^{2+} + HPO_4^{2-} + \cdot 3H_2O \longrightarrow MgHPO_4 \cdot 3H_2O \quad \text{(eq 14)}$$

$$Mg^{2+} + HPO_4^{2-} + \cdot 7H_2O \longrightarrow MgHPO_4 \cdot 7H_2O \quad \text{(eq 15)}$$

$$3Ca^{2+} + 2PO_4^{2-} \longrightarrow Ca_3(PO_4)_2 \quad \text{(eq 16)}$$

$$Ca^{2+} + HPO_4^{2-} \longrightarrow CaHPO_4 \quad \text{(eq 17)}$$

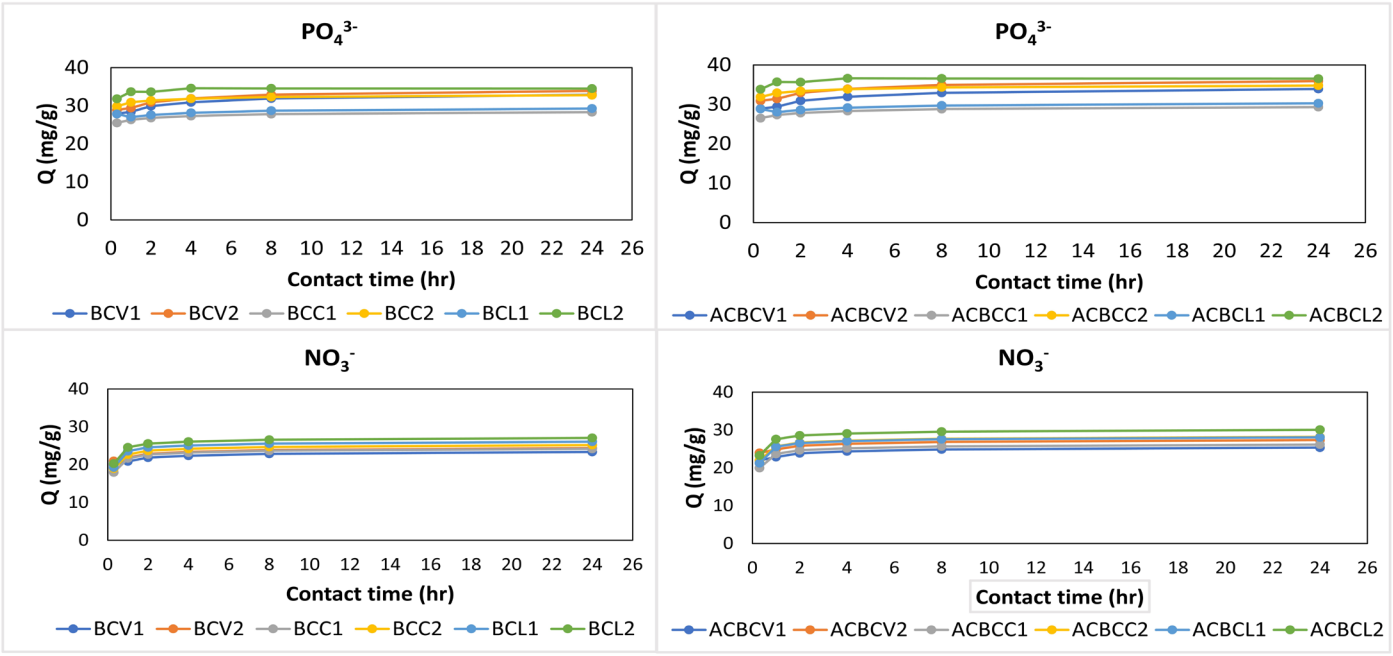

Figure 4. Effect of contact time on PO_4^{3-} and NO_3^- adsorption **by ordinary and activated biochars derived from phytoremediation biomasses**. Q: adsorption capacity,
BCV1: *Chrysopogon zizanioides* non-phytoremediation biochar, BCV2: *Chrysopogon zizanioides* phytoremediation biochar,
BCC1: *Cymbopogon nardus* non-phytoremediation biochar, BCC2: *Cymbopogon nardus* phytoremediation biochar,
BCL1: *Cymbopogon citratus* non-phytoremediation biochar, BCL2: *Cymbopogon citratus* phytoremediation biochar,
ACBCV1: activated *Chrysopogon zizanioides* non-phytoremediation biochar, ACBCV2: activated *Chrysopogon zizanioides* phytoremediation biochar,
ACBCC1: activated *Cymbopogon nardus* non-phytoremediation biochar, ACBCC2: activated *Cymbopogon nardus* phytoremediation biochar,
ACBCL1: activated *Cymbopogon citratus* non-phytoremediation biochar, ACBCL2: activated *Cymbopogon citratus* phytoremediation biochar.

In this current study, the primary adsorption mechanism by phytoremediation biochars was related to their higher surface area and the electrostatic attraction process at solution pH values lower than the pH_{pzc} value of each biochar sample. The high PO_4^{3-} and NO_3^- ions adsorption capacities displayed by biochars from phytoremediation biomasses are partly attributed to their higher surface area compared to non-phytoremediation biochars, as reported in Table 2. Adsorbents with a high surface area tend to have a higher removal capacity for the adsorbate (Gupta and Khatri 2017).

Solution pH is an important factor in adsorption experiments, since it affects the surface charge density, diffusion rate, chemical speciation of the adsorbate, and the protonation and deprotonating of adsorbent surface functional groups (Hafshejani et al. 2016). Figure 4 shows that the adsorption of PO_4^{3-} and NO_3^- ions by ordinary and activated forms of phytoremediation and non-phytoremediation biochars increased as solution pH decreased. Generally, biochars reached optimum adsorption of PO_4^{3-} and NO_3^- ions at a solution pH of 4 and maximum adsorption at a solution pH of 2. BCL2 showed the highest adsorption capacity for PO_4^{3-} ions (28.67 mg g^{-1}) and NO_3^- ions (23.51 mg g^{-1}). The adsorption capacities of ordinary non-phytoremediation biochars for PO_4^{3-} ions decreased in the following order: BCL1 (28.72 mg g^{-1}) > BCC1 (27.57 mg g^{-1}) > BCV1 (22.56 mg g^{-1}). For NO_3^- ions, the adsorption capacities ascended in the following order: BCV2 (22.44 mg g^{-1}) < BCC2 (25.65 mg g^{-1}) < BCL2 (26.58 mg g^{-1}). Among all activated biochars, ACBCL2 displayed the highest adsorption capacities for PO_4^{3-} ions (32.97 mg g^{-1}) and NO_3^- ions (29.64 mg g^{-1}) at pH 2.

A decrease in the adsorption of PO_4^{3-} and NO_3^- ions by biochar as the solution pH increases could be attributed to both changes in the surface charge or charge densities of the adsorbate, and the competition effect among the PO_4^{3-}, NO_3^-, and OH^- ions for adsorption sites on biochar surfaces under alkaline conditions (Yin *et al.* 2018). According to Wang et al. (2018), phosphate ions are preferentially adsorbed over nitrate ions due to their higher valency and higher atomic number. Similar to our current study, Hafshejani et al. (2016) observed minimal PO_4^{3-} and NO_3^- adsorption when solution pH was greater than the point zero charge, as a result of electrostatic repulsion between negatively charged biochar and the PO_4^{3-} and NO_3^- ions. Phosphate ions exist in three forms in water: organic phosphate, condensed phosphate, and orthophosphate (Priya et al. 2022). Different forms of orthophosphate include H_3PO_4, $H_2PO_4^-$, HPO_4^{2-} and PO_4^{3-} (Boyd 2019). Solution pH governs the degree of ionization of phosphate ions and consequently affects their adsorption (Yao et al. 2011). According to Choi et al. (2019), H_3PO_4, $H_2PO_4^-$, PO_4^{2-} and PO_4^{3-} are predominant at solution pH <2.1, 2.1<pH<7.2, 7.2<pH<12.7 and pH>12.7, respectively. NO_3^- ions are stable across a pH scale of 0 to 14 under strongly oxidizing conditions (Zhao et al. 2016). Previous studies (Ip et al. 2009, Shen et al. 2021, Xia et al. 2020, Xu et al. 2021) have proved that it is possible to have affinity between adsorbate and adsorbent bearing the same charges. Van der Waals forces can overcome electrostatic repulsion forces, thus allowing the attachment of the adsorbate onto the adsorbent matrix (Ip et al. 2009, Egbedina et al. 2021). Dai et al. (2020) observed a decrease in electrostatic attraction from pH 3 to 6, with negative charges on biochar increasing

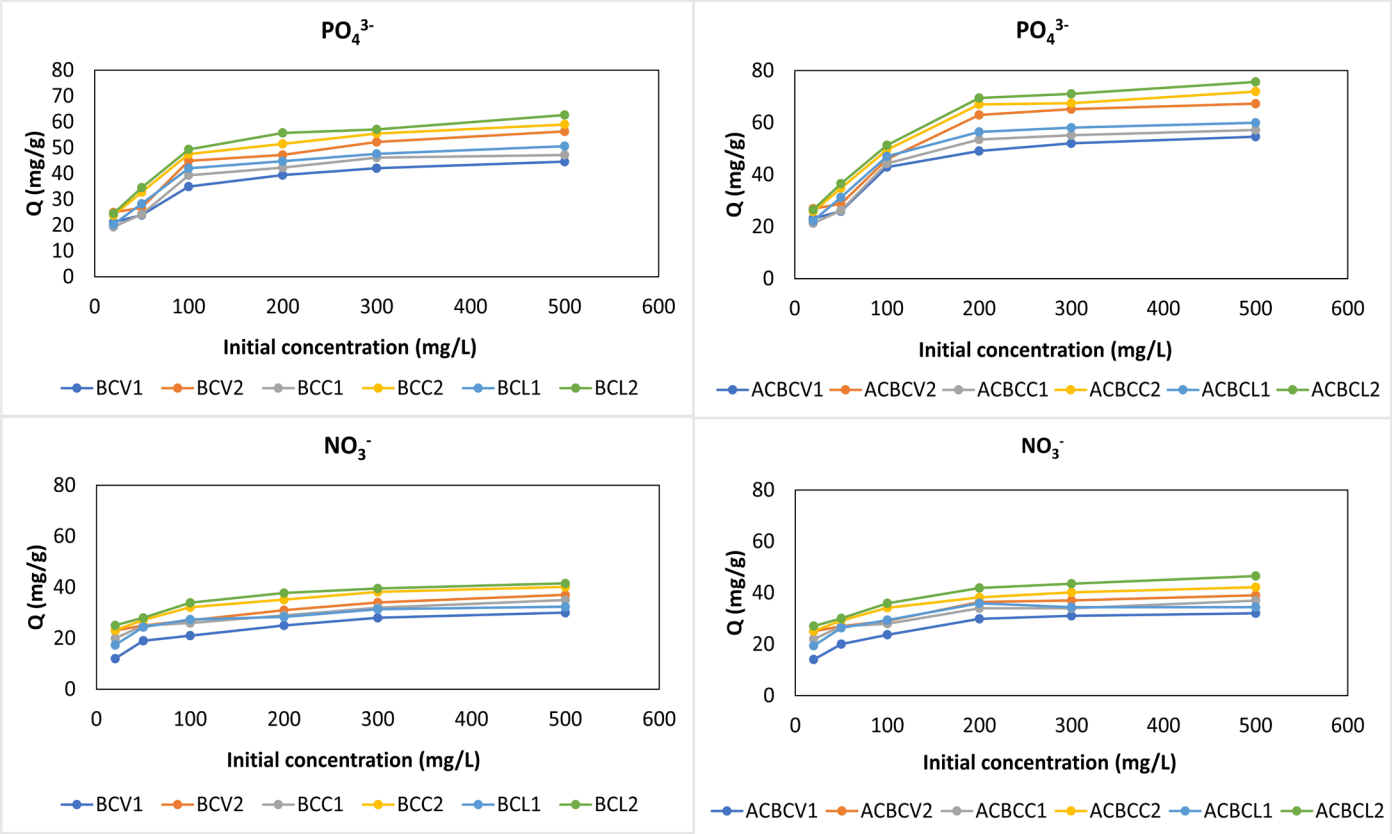

Figure 5. Effect of initial concentration on PO_4^{3-} and NO_3^- adsorption **by ordinary and activated biochars derived from phytoremediation biomasses**. Q: adsorption capacity,
BCV1: *Chrysopogon zizanioides* non-phytoremediation biochar, BCV2: *Chrysopogon zizanioides* phytoremediation biochar,
BCC1: *Cymbopogon nardus* non-phytoremediation biochar, BCC2: *Cymbopogon nardus* phytoremediation biochar,
BCL1: *Cymbopogon citratus* non-phytoremediation biochar, BCL2: *Cymbopogon citratus* phytoremediation biochar,
ACBCV1: activated *Chrysopogon zizanioides* non-phytoremediation biochar, ACBCV2: activated *Chrysopogon zizanioides* phytoremediation biochar,
ACBCC1: activated *Cymbopogon nardus* non-phytoremediation biochar, ACBCC2: activated *Cymbopogon nardus* phytoremediation biochar,
ACBCL1: activated *Cymbopogon citratus* non-phytoremediation biochar, ACBCL2: activated *Cymbopogon citratus* phytoremediation biochar.

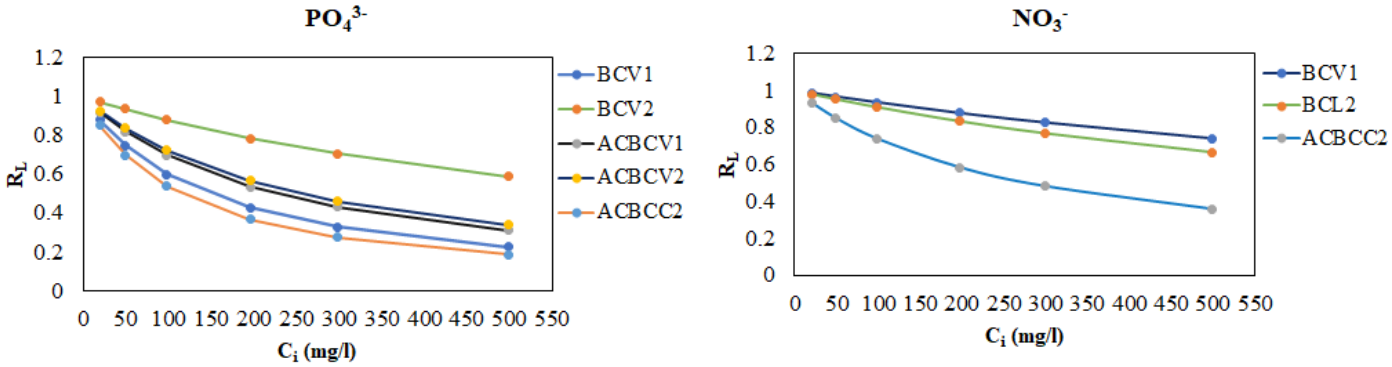

Figure 6. Separation factors versus PO_4^{3-} and NO_3^- initial concentrations of ordinary and activated biochars from non-phytoremediation and phytoremediation biomass. Ci: initial concentration,
BCV1: *Chrysopogon zizanioides* non-phytoremediation biochar, BCV2: *Chrysopogon zizanioides* phytoremediation biochar,
BCL2: *Cymbopogon citratus* phytoremediation biochar, ACBCV1: activated *Chrysopogon zizanioides* non-phytoremediation biochar,
ACBCV2: activated *Chrysopogon zizanioides* phytoremediation biochar, ACBCC2: activated *Cymbopogon nardus* phytoremediation biochar.

above solution pH 6, where ion exchange became the main mechanism for NO_3^- ion adsorption.

The contact time required to reach equilibrium is a crucial factor to consider when estimating the feasibility and efficacy of an adsorbent during pollution removal (Mishra et al. 2014). Figure 5 shows that adsorption by both ordinary and activated biochars increased sharply during the initial time period. The adsorption process reached equilibrium at a contact time of 1 hour. Rapid adsorption of PO_4^{3-} and NO_3^- ion between 0.3 and 1h of contact time is attributed to the availability of active adsorption sites on the biochar surface (Hafshejani et al. 2016). The lack of significant changes in adsorption capacities with

further increases in contact time indicates that the adsorbates have occupied all adsorption sites, or equilibrium has been achieved (Mishra et al. 2014). Generally, the adsorption of PO_4^{3-} and NO_3^- ions by both ordinary phytoremediation and non-phytoremediation biochars increased as the initial concentrations of PO_4^{3-} and NO_3^- ions increased (see Figure 6). Ordinary and activated biochars reached optimum adsorption of PO_4^{3-} and NO_3^- ions at initial concentrations of 300 and 200 mg L^{-1}, respectively. ACBCL2 exhibited the highest adsorption capacities for PO_4^{3-} (75.67 mg g^{-1}) and NO_3^- (46.53 mg g^{-1}) ions at an initial concentration of 500 mg g^{-1}. These results were higher than the PO_4^{3-} ion adsorption capacity (22.03 mg g^{-1})

Table 4. Adsorption isotherm constants of PO_4^{3-} and NO_3^- removal

PO_4^{3-} adsorption												
Isotherm model	**BCV1**	**BCV2**	**BCC1**	**BCC2**	**BCL1**	**BCL2**	**ACBCV1**	**ACBCV2**	**ACBCC1**	**ACBCC2**	**ACBCL1**	**ACBCL2**
Langmuir: linear form 1												
q_m (mg/g)	62.99	72.99					113.64	115.70				
K_L (L/mg)	0.01	0.00					0.00	0.00				
R^2	0.98	0.86					1.00	1.00				
Langmuir: linear form 2												
q_m (mg/g)										101.74		
K_L (L/mg)										0.01		
R^2										0.67		
Temkin												
b_T (L/mg)				61.38	135.05	123.07					264.73	270.59
A_T (J/mol)				0.00	0.00	0.00					0.00	0.00
R^2				0.97	0.32	0.98					0.70	0.90
Dubinin-Radushkevich												
q_m (mg/g)			51.37						46.31			
B_D (mol^2/kJ^2)			0.00						0.00			
R^2			0.96						0.92			
NO_3^- adsorption												
Langmuir: linear form 2												
q_m (mg/g)	317.71					103.23				99.42		
K_L (L/mg)	0.00					0.00				0.01		
R^2	1					1.0				0.67		
Temkin												
b_T (J/mol)		100.81		101.39	125.78		106.00	117.71	110.19			
A_T (L/mg)		0.00		0.00	0.00		0.00	0.00	0.00			
R^2		0.79		0.97	0.33		0.93	0.94	0.97			
Dubinin-Radushkevich												
q_m (mg/g)			57.41								146.18	155.78
B_D (mol^2/kJ^2)			0.00								0.00	0.00
R^2			0.99								0.98	0.91

Note: R^2 is the Regression coefficient, q_m is maximum adsorption capacity, b_T: is the constant related to the heat of adsorption, K_L, A_T, and B_D are the Langmuir constant, Temkin isotherm equilibrium binding constant, and Dubinin-Radushkevich constant of adsorption energy.
BCV1: Chrysopogon *zizanioides* non-phytoremediation biochar, BCV2: *Chrysopogon zizanioides* phytoremediation biochar,
BCC1: *Cymbopogon nardus* non-phytoremediation biochar,
BCL1: *Cymbopogon citratus*, non-phytoremediation biochar, BCL2: *Cymbopogon citratus* phytoremediation biochar,
ACBCV1: activated *Chrysopogon zizanioides* non-phytoremediation biochar, ACBCV2: activated *Chrysopogon zizanioides* phytoremediation biochar,
ACBCC1: activated *Cymbopogon nardus* non-phytoremediation biochar, ACBCC2: activated *Cymbopogon nardus* phytoremediation biochar,
ACBCL1: activated *Cymbopogon citratus* non-phytoremediation biochar, ACBCL2: activated *Cymbopogon citratus* phytoremediation biochar.

of $ZnCl_2$-activated biochar from the water hyacinth plant and the NO_3^- adsorption capacity (10.20 mg g^{-1}) of $ZnCl_2$- activated biochar from coconut granules (Mosa et al. 2018, Li et al. 2019).

The obtained findings align with the phenomenon that adsorption increases with an increasing initial concentration of the adsorbate (Elaigwu et al. 2010). A continuous increase in the initial concentration results in more molecules being available for adsorption at the active sites on the adsorbent's surface (Elaigwu et al. 2010). This, in turn, increases the adsorption capacity until saturation of the adsorption sites. Increasing the initial concentration of the adsorbate also increases the concentration gradient between the solution and the adsorbent, resulting in better mass transfer (Milmile et al. 2011). The rapid uptake of PO_4^{3-} and NO_3^- ions at low concentrations is attributed to the higher surface area available on the biochar surface for the adsorption of fewer PO_4^{3-} and NO_3^- ion species (Berkessa et al. 2019). In chemisorption, where adsorption occurs at higher initial concentrations of PO_4^{3-} and NO_3^- ions , monolayer adsorption is attained, preventing further removal of PO_4^{3-} and NO_3^- ions by the biochar surfaces (Sayadi et al. 2020). The biochars reached optimum adsorption at initial concentrations of 300 for PO_4^{3-} ions and 200 mg L^{-1} for NO_3^- ions, with activated biochars displaying higher adsorption capacities compared to ordinary biochars. This could be attributed to their improved adsorption characteristics, such as highly porous structures, high surface area, pore size, and volume, as shown in Figure 2 and Table 2.

Adsorption isotherms of PO_4^{3-} and NO_3^- ions in a binary system

The highest regression coefficients (R^2) (results shown in Tables S2a and S2b) indicate that the sample best fits a particular adsorption isotherm. BCV1, BCV2, BCC2, BCL2, ACBCV1, ACBCV2, ACBCC2, and ACBCL2 best fitted the Langmuir adsorption model (linear form 1 or 2) during PO_4^{3-} ion adsorption, as shown in Table S2a. BCC2, BCL1, and ACBCL1 best fitted the Temkin adsorption model, while BCC1 and ACBCC1 best fitted the Dubinin-Radushkevich adsorption model during PO_4^{3-} ion adsorption. During NO_3^- ion adsorption, BCV1, BCC2, BCL2, ACBCV1, ACBCV2 and ACBCC2 best fitted the Langmuir model (linear form 1 or 2), as shown in Table S2b. BCC2, BCL1, and ACBCC1 best fitted the Temkin adsorption model, while BCC1, ACBCL1, and ACBCL2 best followed the Dubinin-Radushkevich adsorption model during NO_3^- adsorption. A high regression coefficient is an indication of strong adsorption between the adsorbate and the adsorbent (Kabbashi et al. 2009).

It was observed that the maximum adsorption capacities (q_m) for PO_4^{3-} ions by BCV1, BCV2, ACBCV1, ACBCV2, and ACBCC2 are 62.99, 72.99, 113.64, 115.70, and 61.38 mg g^{-1}, respectively (see Table 4). The q_m values for NO_3^- ion adsorption by BCV1, BCL2, and ACBCC2 are 317.71, 294.7, and 99.42 mg g^{-1}, respectively. The Langmuir equation describes the adsorption of adsorbate(s) by homogeneous surfaces via chemical mechanisms (chemisorption) (Yin et al. 2018). The Temkin adsorption isotherm was followed by BCC2, BCL1, BCL2, ACBCL1, and ACBCL2 during PO_4^{3-} ion adsorption, with possible maximum adsorptions at 61.38, 135.05, 123.07, 264.73, and 146.15 L g^{-1}, respectively. BCV2, BCC2, BCL1, ACBCV1, BCV2, and BCC1 best fitted the Temkin adsorption equation for NO_3^- ion adsorption. The Temkin adsorption isotherm considers the indirect adsorbate interactions and explains that there is a linear decrease in the heat of adsorption of all molecules in the layer as coverage increases (Lalley et al. 2016). The Dubinin-Radushkevich adsorption isotherm was followed by BCC1 and ACBCC1 for PO_4^{3-} ion adsorption, while for NO_3^- ions adsorption, the model was followed by BCC1, ACBCL2 (see Table 4). The maximum PO_4^{3-} ion adsorption capacities by BCC1 and activated BCC1 were found to be 51.37 and 46.31 mg g^{-1}, respectively. The maximum adsorption capacities of BCC1, ACBCL1, and ACBCL2 were 57.41, 146.18, and 155.78 mg g^{-1}, respectively. The Dubinin-Radushkevich adsorption isotherm explains the physical deposition of adsorbate on the adsorbent structure (Banu et al. 2020).

The K_L (Langmuir adsorption constant) represents the strength of adsorption. The values in Table 5 indicate weak adsorption strength, with K_L values ranging between 0.007 and 0.046 L mg^{-1}. Figure 6 shows the separation fac tor (R_L) values ranging from 0 to 1 for both PO_4^{3-} and NO_3^- ions adsorption. The graphs indicate a decreasing trend in the separation factor with increasing initial concentrations of PO_4^{3-} and NO_3^- ions. The separation factor graphs for PO_4^{3-} ion adsorption descended in the following order: BCV1>ACBCV2> ACBCV1> BCV1>ACBCC2. For nitrate ion adsorption, the separation factor versus initial concentration decreased in the following order: BCV1> BCL2> ACBCC2. The uptake of adsorbate by the adsorbent is determined by the separation factor constant (R_L) (Temkin and Acikel 2022). The adsorption isotherm is considered appropriate or favorable if the R_L values range between 0 and 1. The decrease in the separation factor with increasing initial concentration of the adsorbate implies that the adsorption is more favorable at higher concentrations (Chen et al. 2017). The heat of adsorption (K_T) constant from the Temkin adsorption model ranged from 0.006 to 0.024. Nandiyanto et al. (2020) associated low K_T values with minimal binding energy between the adsorbent and the adsorbate. B_D refers to the free energy of adsorption as the adsorbate diffuses from the bulk solution onto the adsorbent's surface (Olalekan et al. 2013). B_D values from Dubinin-Radushkevich adsorption isotherm ranged between 0.001 and 0.004 mol^2/kJ^2.

Conclusion

In conclusion, phytoremediation biochars displayed more porous structures, higher specific surface areas, and greater pore volumes compared to non-phytoremediation biochars. The pore sizes of ordinary phytoremediation and non-phytoremediation biochars ranged from 0.02 to 0.08 nm and from 0.04 to 0.12 nm, respectively. These parameters were further enhanced after the activation of ordinary biochars using $ZnCl_2$. All biochar samples used in this study were protonated, and the point of zero charge values of the activated biochars was lower than that of ordinary biochars. Among the biochars, ACBCL2 displayed higher PO_4^{3-} and NO_3^- ion adsorption capacities compared to ACBCC2 and ACBCV2. Specifically, ACBCV2, ACBCC2, and ACBCL2 could remove 115.70, 101.74, and 270.59 mg g^{-1} of phosphate ions from wastewater, respectively. Additionally, ACBCL2, ACBCC2, and ACBCV2 could remove 155.78, 99.42, and 117.71 mg g^{-1} of nitrate ions from

wastewater, respectively. This study recommends exploring different activation reagents to enhance net positive charges on phytoremediation biochar surfaces, thereby maximizing their potential for adsorption anionic contaminants in wastewater. Different impregnations could be investigated during the activation process to identify the best impregnation ratio that could help in optimizing the adsorption of oppositely charged adsorbate. The mechanisms of adsorption of adsorbates onto adsorbent matrices bearing the same charges should be further studied.

Acknowledgments

This study was financially supported by the Botswana International University of Science and Technology under the Postgraduate Initiation Grant, grant number S00357, awarded to KLS, and the AJ Core Project under the Ministry of Tertiary Education, Research, Science and Technology-Department of Research, Science, and Technology (DRST), awarded to VUU. It was also partially supported by JST Strategic International Collaborative Research Program (SCIORP), grant number JPMJSC22A2, Japan. We would like to thank Professor Masaki Takaoka (Kyoto University) for supporting this research.

Competing Interest

There is no competing interest declared by the authors.

Author Contributions

All authors contributed to sample collection, data generation and analysis, and compilation of the manuscript. All authors revised and approved the final manuscript.

Data Availability

No other data is associated with this manuscript.

References

Abd Rahman, A. A., Alias, A. B., Jaffar, N. N. & Amir, M. A. (2019). Adsorption of hydrogen sulphide by commercialized rice husk biochar (RHB) & hydrogel biochar composite (RH-HBC). *Int. J. Recent Technol. Eng*, 8(4), pp. 6864-6870. DOI:10.35940/ijrte.D5207.118419.

Ahmed, M. B., Zhou, J. L., Ngo, H. H., Guo, W. & Chen, M. (2016). Progress in the preparation and application of modified biochar for improved contaminant removal from water and wastewater. *Bioresource technology*, 214, pp. 836-851. DOI:10.1016/j.biortech.2016.05.057.

Alagha, O., Manzar, M. S., Zubair, M., Anil, I., Mu'azu, N. D. & Qureshi, A. (2020). Comparative adsorptive removal of phosphate and nitrate from wastewater using biochar-MgAl LDH nanocomposites: coexisting anions effect and mechanistic studies. *Nanomaterials*, 10(2), 336. DOI:10.3390/nano10020336.

Angın, D., Altintig, E. & Köse, T. E. (2013). Influence of process parameters on the surface and chemical properties of activated carbon obtained from biochar by chemical activation. *Bioresource Technology*, 148, pp. 542-549. DOI: 10.1016/j.biortech.2013.08.164.

Banu, H. A. T., Karthikeyan, P., Vigneshwaran, S. & Meenakshi, S. (2020). Adsorptive performance of lanthanum encapsulated biopolymer chitosan-kaolin clay hybrid composite for the recovery of nitrate and phosphate from water. *International journal of biological macromolecules*, 154, pp. 188-197. DOI: 10.1016/j.ijbiomac.2020.03.074.

Barquilha, C. E. & Braga, M. C. (2021). Adsorption of organic and inorganic pollutants onto biochars: Challenges, operating conditions, and mechanisms. *Bioresource Technology Reports*, 15, 100728. DOI:10.1016/j.biteb.2021.100728.

Berkessa, Y. W., Mereta, S. T. & Feyisa, F. F. (2019). Simultaneous removal of nitrate and phosphate from wastewater using solid waste from the factory. *Applied Water Science*, 9, pp. 1-10. DOI:10.1007/s13201-019-0906-z.

Biswas, B., Rahman, T., Sakhakarmy, M., Jahromi, H., Eisa, M., Baltrusaitis, J. & Adhikari, S. (2023). Phosphorus adsorption using chemical and metal chloride activated biochars: Isotherms, kinetics and mechanism study. *Heliyon*, 9(9). DOI:10.1016/j.heliyon.2023.e19830.

Borchard, N., Wolf, A., Laabs, V., Aeckersberg, R., Scherer, H. W., Moeller, A. & Amelung, W. (2012). Physical activation of biochar and its meaning for soil fertility and nutrient leaching–a greenhouse experiment. *Soil Use and Management*, 28(2), pp. 177-184. DOI:10.1111/j.1475-2743.2012.00407.x

Bouchemal, N., Belhachemi, M., Merzougui, Z. and Addoun, F. (2009). The effect of temperature and impregnation ratio on the active carbon porosity. *Desalination and water treatment*, 10(1-3), pp.115-120. DOI:10.5004/dwt.2009.828.

Boyd, C. E. (2019). *Water quality: an introduction*. Springer Nature. DOI 10.1007/978-3-319-17446-4.

Buentello-Montoya, D., Zhang, X., Li, J., Ranade, V., Marques, S. & Geron, M. (2020). Performance of biochar as a catalyst for tar steam reforming: Effect of the porous structure. *Applied energy*, 259, 114176. DOI:10.1016/j.apenergy.2019.114176.

Chen, C., Fu, Y., Yu, L. L., Li, J. & Li, D. Q. (2017). Removal of methylene blue by seed-watermelon pulp-based low-cost adsorbent: Study of adsorption isotherms and kinetic models. *Journal of Dispersion Science and Technology*, 38(8), pp. 1142-1146. DOI:10.1080/01932691.2016.1225263.

Choi, Y. K., Jang, H. M., Kan, E., Wallace, A. R. & Sun, W. (2019). Adsorption of phosphate in water on a novel calcium hydroxide-coated dairy manure-derived biochar. *Environmental Engineering Research*, 24(3), pp. 434-442. DOI:10.4491/eer.2018.296.

Dai, Y., Wang, W., Lu, L., Yan, L. & Yu, D. (2020). Utilization of biochar for the removal of nitrogen and phosphorus. *Journal of Cleaner Production*, 257, 120573. DOI:10.1016/j.jclepro.2020.120573.

Deng, Y., Li, M., Zhang, Z., Liu, Q., Jiang, K., Tian, J. & Ni, F. (2021). Comparative study on characteristics and mechanism of phosphate adsorption on Mg/Al modified biochar. *Journal of Environmental Chemical Engineering*, 9(2), 105079. DOI:10.1016/j.jece.2021.105079.

Du, J., Zhang, L., Liu, T., Xiao, R., Li, R., Guo, D. & Zhang, Z. (2019). Thermal conversion of a promising phytoremediation plant (Symphytum officinale L.) into biochar: dynamic of potentially toxic elements and environmental acceptability assessment of the biochar. *Bioresource technology*, 274, pp. 73-82. DOI:10.1016/j.biortech.2018.11.077.

Egbedina, A. O., Adebowale, K. O., Olu-Owolabi, B. I., Unuabonah, E. I. & Adesina, M. O. (2021). Green synthesis of ZnO coated hybrid biochar for the synchronous removal of ciprofloxacin and

tetracycline in wastewater. *RSC advances*, 11(30), pp. 18483-18492. DOI: 10.1039/d1ra01130h.

Elaigwu, S. E., Usman, L. A., Awolola, G. V., Adebayo, G. B. & Ajayi, R. M. K. (2010). Adsorption of Pb (II) from aqueous solution by activated carbon prepared from cow dung. *Environmental Research Journal*, 4(4), pp. 257-260.

Feng, Q., Chen, M., Wu, P., Zhang, X., Wang, S., Yu, Z. & Wang, B. (2022). Simultaneous reclaiming phosphate and ammonium from aqueous solutions by calcium alginate-biochar composite: Sorption performance and governing mechanisms. *Chemical Engineering Journal*, 429, 132166. DOI:10.1016/j.cej.2021.132166.

Foo, K. Y. & Hameed, B. H. (2010). Insights into the modeling of adsorption isotherm systems. *Chemical engineering journal*, 156(1), pp. 2-10. DOI:10.1016/j.cej.2009.09.013.

Gámiz, B., Hall, K., Spokas, K. A. & Cox, L. (2019). Understanding activation effects on low-temperature biochar for optimization of herbicide sorption. *Agronomy*, 9(10), 588. DOI: 10.3390/agronomy9100588.

Ghosh, M. & Singh, S. P. (2005). A review on phytoremediation of heavy metals and utilization of it's by products. *Asian J Energy Environ*, 6(4), 18.

Gizaw, A., Zewge, F., Kumar, A., Mekonnen, A. & Tesfaye, M. (2021). A comprehensive review on nitrate and phosphate removal and recovery from aqueous solutions by adsorption. *AQUA—Water Infrastructure, Ecosystems and Society*, 70(7), pp. 921-947. DOI:10.2166/aqua.2021.146.

Gray, M., Johnson, M. G., Dragila, M. I. & Kleber, M. (2014). Water uptake in biochars: The roles of porosity and hydrophobicity. *Biomass and bioenergy*, 61, pp. 196-205.

Guo, F., Peng, K., Liang, S., Jia, X., Jiang, X. & Qian, L. (2019). Evaluation of the catalytic performance of different activated biochar catalysts for removal of tar from biomass pyrolysis. *Fuel*, 258, 116204. DOI:10.1016/j.biombioe.2013.12.010.

Gupta, K. & Khatri, O. P. (2017). Reduced graphene oxide as an effective adsorbent for removal of malachite green dye: Plausible adsorption pathways. *Journal of colloid and interface science*, 501, pp. 11-21. DOI:10.1016/j.jcis.2017.04.035.

Hafshejani, L. D., Hooshmand, A., Naseri, A. A., Mohammadi, A. S., Abbasi, F. & Bhatnagar, A. (2016). Removal of nitrate from aqueous solution by modified sugarcane bagasse biochar. *Ecological Engineering*, 95, pp. 101-111. DOI: 10.1016/j.ecoleng.2016.06.035.

He, J., Strezov, V., Kumar, R., Weldekidan, H., Jahan, S., Dastjerdi, B. H. & Kan, T. (2019). Pyrolysis of heavy metal contaminated Avicennia marina biomass from phytoremediation: Characterisation of biomass and pyrolysis products. *Journal of Cleaner Production*, 234, 1235-1245. DOI:10.1016/j.jclepro.2019.06.285.

He, J., Strezov, V., Zhou, X., Kumar, R. & Kan, T. (2020). Pyrolysis of heavy metal contaminated biomass pre-treated with ferric salts: Product characterisation and heavy metal deportment. *Bioresource Technology*, 313, 123641. DOI:10.1016/j.biortech.2020.123641.

Hock, P. E. & Zaini, & M. A. A. (2018). Activated carbons by zinc chloride activation for dye removal–a commentary. *Acta chimica slovaca*, *11*(2), pp. 99-106. DOI: 0.2478/acs-2018-0015.

Huang, Y., Chu, H., Wang, D. & Hui, S. (2024). Performance and mechanism of benzene adsorption on $ZnCl_2$ one-step modified corn cob biochar. *Environmental Science and Pollution Research*, 31(10), pp. 15209-15222. DOI: 10.1007/s11356-024-32183-7.

Hung, C. Y., Tsai, W. T., Chen, J. W., Lin, Y. Q. & Chang, Y. M. (2017). Characterization of biochar prepared from biogas digestate. *Waste management*, 66, pp. 53-60. DOI:10.1016/j.wasman.2017.04.034.

Inyang, M. I., Gao, B., Yao, Y., Xue, Y., Zimmerman, A., Mosa, A. & Cao, X. (2016). A review of biochar as a low-cost adsorbent for aqueous heavy metal removal. *Critical Reviews in Environmental Science and Technology*, 46(4), pp. 406-433. DOI:10.1080/10643389.2015.1096880.

Ip, A. W. M., Barford, J. P. & McKay, G. (2009). Reactive Black dye adsorption/desorption onto different adsorbents: effect of salt, surface chemistry, pore size and surface area. *Journal of colloid and interface science*, 337(1), pp. 32-38. DOI:10.1016/j.jcis.2009.05.015.

Itodo, A. U., Itodo, H. U. & Gafar, M. K. (2010). Estimation of specific surface area using Langmuir isotherm method. *Journal of Applied Sciences and Environmental Management*, 14(4). DOI:10.4314/jasem.v14i4.63287.

Jing, X. R., Wang, Y. Y., Liu, W. J., Wang, Y. K. & Jiang, H. (2014). Enhanced adsorption performance of tetracycline in aqueous solutions by methanol-modified biochar. *Chemical Engineering Journal*, 248, pp. 168-174. DOI:10.1016/j.cej.2014.03.006.

Kabbashi, N. A., Atieh, M. A., Al-Mamun, A., Mirghami, M. E., Alam, M. D. Z. & Yahya, N. (2009). Kinetic adsorption of application of carbon nanotubes for Pb (II) removal from aqueous solution. *Journal of Environmental Sciences*, 21(4), pp. 539-544. DOI:10.1016/S1001-0742(08)62305-0.

Lalley, J., Han, C., Li, X., Dionysiou, D. D. & Nadagouda, M. N. (2016). Phosphate adsorption using modified iron oxide-based sorbents in lake water: kinetics, equilibrium, and column tests. *Chemical Engineering Journal,* 284, pp. 1386-1396. DOI:10.1016/j.cej.2015.08.114.

Lawal, A. A., Hassan, M. A., Zakaria, M. R., Yusoff, M. Z. M., Norrrahim, M. N. F., Mokhtar, M. N. & Shirai, Y. (2021). Effect of oil palm biomass cellulosic content on nanopore structure and adsorption capacity of biochar. *Bioresource Technology*, 332, 125070. DOI:10.1016/j.biortech.2021.125070.

Lee, H. S. & Shin, H. S. (2021). Competitive adsorption of heavy metals onto modified biochars: Comparison of biochar properties and modification methods. *Journal of Environmental Management*, 299, 113651. DOI:10.1016/j.jenvman.2021.113651.

Lee, S. Y. & Park, S. J. (2013). Determination of the optimal pore size for improved CO_2 adsorption in activated carbon fibers. *Journal of colloid and interface science*, 389(1), pp. 230-235. DOI:10.1016/j.jcis.2012.09.018.

Li, B., Hu, J., Xiong, H. & Xiao, Y. (2020). Application and properties of microporous carbons activated by $ZnCl_2$: adsorption behavior and activation mechanism. *ACS omega*, 5(16), pp. 9398-9407. DOI:10.1021/acsomega.0c00461.

Li, X., Zhao, C. & Zhang, M. (2019). Biochar for anionic contaminants removal from water. In *Biochar from biomass and waste* pp. 143-160. Elsevier. DOI:10.1016/B978-0-12-811729-3.00008-X.

Liu, A., Chen, J., Lu, X., Li, D. & Xu, W. (2021). Influence of components interaction on pyrolysis and the explosion of biomass dust. *Process Safety and Environmental Protection*, *154*, pp. 384-392. DOI:10.1016/j.psep.2021.08.032.

Liu, L., Ji, M. & Wang, F. (2018). Adsorption of nitrate onto $ZnCl_2$-modified coconut granular activated carbon: kinetics, characteristics, and adsorption dynamics. *Advances in Materials Science and Engineering*, DOI:10.1155/2018/1939032.

Liu, N., Charrua, A. B., Weng, C. H., Yuan, X. & Ding, F. (2015). Characterization of biochars derived from agriculture wastes and their adsorptive removal of atrazine from aqueous solution: A comparative study. *Bioresource technology*, 198, pp. 55-62. DOI:10.1016/j.biortech.2015.08.129.

Liu, W. J., Tian, K., Jiang, H. & Yu, H. Q. (2014). Harvest of Cu NP anchored magnetic carbon materials from Fe/Cu preloaded biomass: their pyrolysis, characterization, and catalytic activity on aqueous reduction of 4-nitrophenol. *Green chemistry*, 16(9), pp. 4198-4205. DOI:10.1039/C4GC00599F.

Machado, L. M., Lütke, S. F., Perondi, D., Godinho, M., Oliveira, M. L., Collazzo, G. C. & Dotto, G. L. (2020). Treatment of effluents containing 2-chlorophenol by adsorption onto chemically and physically activated biochars. *Journal of Environmental Chemical Engineering*, 8(6), 104473. DOI:10.1016/j.jece.2020.104473.

Majd, M. M., Kordzadeh-Kermani, V., Ghalandari, V., Askari, A. & Sillanpää, M. (2022). Adsorption isotherm models: A comprehensive and systematic review (2010− 2020). *Science of The Total Environment*, 812, 151334. DOI:10.1016/j.scitotenv.2021.151334.

Mehdizadeh, S., Sadjadi, S., Ahmadi, S. J. & Outokesh, M. (2014). Removal of heavy metals from aqueous solution using platinum nanopartcles/Zeolite-4A. *Journal of Environmental Health Science and Engineering*, 12, pp. 1-7.

Menya, E., Olupot, P. W., Storz, H., Lubwama, M. & Kiros, Y. (2018). Production and performance of activated carbon from rice husks for removal of natural organic matter from water: a review. *Chemical Engineering Research and Design*, 129, pp. 271-296. DOI:10.1016/j.cherd.2017.11.008.

Milmile, S. N., Pande, J. V., Karmakar, S., Bansiwal, A., Chakrabarti, T. & Biniwale, R. B. (2011). Equilibrium isotherm and kinetic modeling of the adsorption of nitrates by anion exchange Indion NSSR resin. *Desalination*, 276(1-3), pp. 38-44. DOI:10.1016/j.desal.2011.03.015.

Mishra, S. P., Mohapatra, D., Mishra, D., Chattopadhyay, P., Chaudhury, G. R. & Das, R. P. (2014). Arsenic adsorption on natural minerals. *J Mater Environ Sci*, 5(2), pp. 350-359.

Mosa, A., El-Ghamry, A. & Tolba, M. (2018). Functionalized biochar derived from heavy metal-rich feedstock: phosphate recovery and reusing the exhausted biochar as an enriched soil amendment. *Chemosphere*, *198*, pp. 351-363. DOI:10.1016/j.chemosphere.2018.01.113.

Muzyka, R., Misztal, E., Hrabak, J., Banks, S. W. & Sajdak, M. (2023). Various biomass pyrolysis conditions influence the porosity and pore size distribution of biochar. *Energy*, 263, 126128. DOI:10.1016/j.energy.2022.126128.

Nandiyanto, A. B. D., Arinalhaq, Z. F., Rahmadianti, S., Dewi, M. W., Rizky, Y. P. C., Maulidina, A. & Yunas, J. (2020). Curcumin Adsorption on Carbon Microparticles: Synthesis from Soursop (AnnonaMuricata L.) Peel Waste, Adsorption Isotherms and Thermodynamic and Adsorption Mechanism. *International Journal of Nanoelectronics & Materials*, 13.

Olalekan, A. P., Dada, A. O. & Okewale, A. O. (2013). Comparative adsorption isotherm study of the removal of Pb^{2+} and Zn^{2+} onto agricultural waste. *Res. J. Chem. Environ. Sci*, 1, pp. 22-27.

Paredes-Laverde, M., Salamanca, M., Diaz-Corrales, J. D., Flórez, E., Silva-Agredo, J. & Torres-Palma, R. A. (2021). Understanding the removal of an anionic dye in textile wastewaters by adsorption on $ZnCl_2$ activated carbons from rice and coffee husk wastes: A combined experimental and theoretical study. *Journal of Environmental Chemical Engineering*, 9(4), 105685. DOI:10.1016/j.jece.2021.105685.

Pena, J., Villot, A. & Gerente, C. (2020). Pyrolysis chars and physically activated carbons prepared from buckwheat husks for catalytic purification of syngas. *Biomass and bioenergy*, 132, 105435. DOI:10.1016/j.biombioe.2019.105435.

Priya, E., Kumar, S., Verma, C., Sarkar, S. & Maji, P. K. (2022). A comprehensive review on technological advances of adsorption for removing nitrate and phosphate from wastewater. *Journal of Water Process Engineering*, 49, 103159. DOI:10.1016/j.jwpe.2022.103159.

Sayadi, M., Farasati, M., G Mahmoodlu, M. & Rostami Charati, F. (2020). Removal of nitrate, ammonium, and phosphate from water using conocarpus and paulownia plant biochar. *Iranian Journal of Chemistry and Chemical Engineering*, 39(4), pp. 205-222.

Sefatlhi, K. L., Ultra Jr, V. U. & Majoni, S. (2024). Chemical and Structural Characteristics of Biochars from Phytoremediation Biomass of Cymbopogon Citratus, Cymbopogon Nardus, and Chrysopogon Zizanioides. *Waste and Biomass Valorization*, 15(1), pp. 283-300. DOI:10.1007/s12649-023-02164-x.

Shen, M., Song, B., Zeng, G., Zhang, Y., Teng, F. & Zhou, C. (2021). Surfactant changes lead adsorption behaviors and mechanisms on microplastics. *Chemical Engineering Journal*, 405, 126989.

Tekin, B. & Açikel, U. (2022). Adsorption isotherms for removal of heavy metal ions (copper and nickel) from aqueous solutions in single and binary adsorption processes. *Gazi University Journal of Science*, 36(2), pp. 495-509. DOI:10.35378/gujs.1066137.

Thue, P. S., Lima, D. R., Lima, E. C., Teixeira, R. A., dos Reis, G. S., Dias, S. L. & Machado, F. M. (2022). Comparative studies of physicochemical and adsorptive properties of biochar materials from biomass using different zinc salts as activating agents. *Journal of Environmental Chemical Engineering*, 10(3), 107632. DOI:10.1016/j.jece.2022.107632.

Thue, P. S., Lima, D. R., Lima, E. C., Teixeira, R. A., dos Reis, G. S., Dias, S. L. & Machado, F. M. (2022). Comparative studies of physicochemical and adsorptive properties of biochar materials from biomass using different zinc salts as activating agents. *Journal of Environmental Chemical Engineering*, 10(3), 107632. DOI:10.1016/j.jece.2022.107632.

Ultra, V. U., Ngwako, K. M. & Eliason, P. (2022). Physiological Responses, Growth, and Heavy Metal Accumulation of Citronella (Cymbopogon nardus Rendle.) in Cu-Ni Mine Tailings as Affected by Soil Amendments. *Philippine Journal of Science*, *151*(3). DOI:10.56899/151.03.36.

Wang, L., Xu, Z., Fu, Y., Chen, Y., Pan, Z., Wang, R. & Tan, Z. (2018). Comparative analysis on adsorption properties and mechanisms of nitrate and phosphate by modified corn stalks. *RSC advances*, 8(64), pp. 36468-36476. DOI:10.1039/C8RA06617E.

Wang, T., Zheng, J., Liu, H., Peng, Q., Zhou, H. & Zhang, X. (2021). Adsorption characteristics and mechanisms of Pb^{2+} and Cd^{2+} by a new agricultural waste–Caragana korshinskii biomass derived biochar. *Environmental Science and Pollution Research*, 28, pp. 13800-13818. DOI:10.1007/s11356-020-11571-9.

Wang, Z., Guo, H., Shen, F., Yang, G., Zhang, Y., Zeng, Y. & Deng, S. (2015). Biochar produced from oak sawdust by Lanthanum (La)-involved pyrolysis for adsorption of ammonium (NH_4^+), nitrate (NO_3^-), and phosphate (PO_4^{3-}). *Chemosphere*, 119, pp. 646-653. DOI:10.1016/j.chemosphere.2014.07.084.

Williams, P. T. & Reed, A. R. (2004). High grade activated carbon matting derived from the chemical activation and pyrolysis of

natural fibre textile waste. *Journal of analytical and applied pyrolysis*, 71(2), pp. 971-986. DOI:10.1016/j.jaap.2003.12.007.

Wu, B., Wan, J., Zhang, Y., Pan, B. & Lo, I. M. (2019). Selective phosphate removal from water and wastewater using sorption: process fundamentals and removal mechanisms. *Environmental science & technology*, 54(1), pp. 50-66. DOI:10.1021/acs.est.9b05569.

Xia, M., Chen, Z., Li, Y., Li, C., Ahmad, N. M., Cheema, W. A. & Zhu, S. (2019). Removal of Hg (II) in aqueous solutions through physical and chemical adsorption principles. *RSC advances*, 9(36), pp. 20941-20953. DOI:10.1039/C9RA01924C.

Xia, Y., Zhou, J. J., Gong, Y. Y., Li, Z. J. & Zeng, E. Y. (2020). Strong influence of surfactants on virgin hydrophobic microplastics adsorbing ionic organic pollutants. *Environmental Pollution*, 265, 115061. DOI:10.1016/j.envpol.2020.115061.

Xie, T., Reddy, K. R., Wang, C., Yargicoglu, E. & Spokas, K. (2015). Characteristics and applications of biochar for environmental remediation: a review. *Critical Reviews in Environmental Science and Technology*, 45(9), pp. 939-969. DOI:10.1080/10643389.2014.924180.

Xu, D. D., Ma, R. R., Fu, A. P., Guan, Z., Zhong, N., Peng, H. & Duan, C. G. (2021). Ion adsorption-induced reversible polarization switching of a van der Waals layered ferroelectric. *Nature communications*, 12(1), 655. DOI:10.1038/s41467-021-20945-7.

Yağmur, H. K. & Kaya, İ. (2021). Synthesis and characterization of magnetic $ZnCl_2$-activated carbon produced from coconut shell for the adsorption of methylene blue. *Journal of molecular structure*, 1232, 130071. DOI:10.1016/j.molstruc.2021.130071.

Yan, L., Liu, Y., Zhang, Y., Liu, S., Wang, C., Chen, W. & Zhang, Y. (2020). $ZnCl_2$ modified biochar derived from aerobic granular sludge for developed microporosity and enhanced adsorption to tetracycline. *Bioresource Technology*, 297, 122381. DOI:10.1016/j.biortech.2019.122381.

Yang, S., Katuwal, S., Zheng, W., Sharma, B. & Cooke, R. (2021). Capture and recover dissolved phosphorous from aqueous solutions by a designer biochar: Mechanism and performance insights. *Chemosphere*, 274, 129717. DOI:10.1016/j.chemosphere.2021.12

Yao, Y., Gao, B., Inyang, M., Zimmerman, A. R., Cao, X., Pullammanappallil, P. & Yang, L. (2011). Removal of phosphate from aqueous solution by biochar derived from anaerobically digested sugar beet tailings. *Journal of hazardous materials*, 190(1-3), pp. 501-507. DOI:10.1016/j.jhazmat.2011.03.083.

Yao, Y., Gao, B., Zhang, M., Inyang, M. & Zimmerman, A. R. (2012). Effect of biochar amendment on sorption and leaching of nitrate, ammonium, and phosphate in sandy soil. *Chemosphere*, 89(11), pp. 1467-1471. DOI:10.1016/j.chemosphere.2012.06.002.

Yin, Q., Ren, H., Wang, R. & Zhao, Z. (2018). Evaluation of nitrate and phosphate adsorption on Al-modified biochar: influence of Al content. *Science of the Total Environment*, 631, pp. 895-903. DOI:10.1016/j.scitotenv.2018.03.091.

Zhang, M., Song, G., Gelardi, D. L., Huang, L., Khan, E., Mašek, O. & Ok, Y. S. (2020). Evaluating biochar and its modifications for the removal of ammonium, nitrate, and phosphate in water. *Water Research*, 186, 116303. DOI:10.1016/j.watres.2020.116303.

Zhao, B., Xu, X., Xu, S., Chen, X., Li, H. & Zeng, F. (2017). Surface characteristics and potential ecological risk evaluation of heavy metals in the bio-char produced by co-pyrolysis from municipal sewage sludge and hazelnut shell with zinc chloride. *Bioresource technology*, 243, pp. 375-383.DOI:10.1016/j.biortech.2017.06.032.

Zhao, L., Cao, X., Zheng, W., Wang, Q. & Yang, F. (2015). Endogenous minerals have influences on surface electrochemistry and ion exchange properties of biochar. *Chemosphere*, 136, pp. 133-139. DOI:10.1016/j.chemosphere.2015.04.053.

Zhao, S., Zhou, N. & Shen, X. (2016). Driving mechanisms of nitrogen transport and transformation in lacustrine wetlands. *Science China Earth Sciences*, 59, pp. 464-476. DOI:10.1007/s11430-015-5230-3.

Zubir, M. H. M. & Zaini, M. A. A. (2020). Twigs-derived activated carbons via $H_3PO_4/ZnCl_2$ composite activation for methylene blue and congo red dye removal. *Scientific reports*, 10(1), 14050. DOI:10.1038/s41598-020-71034-6.

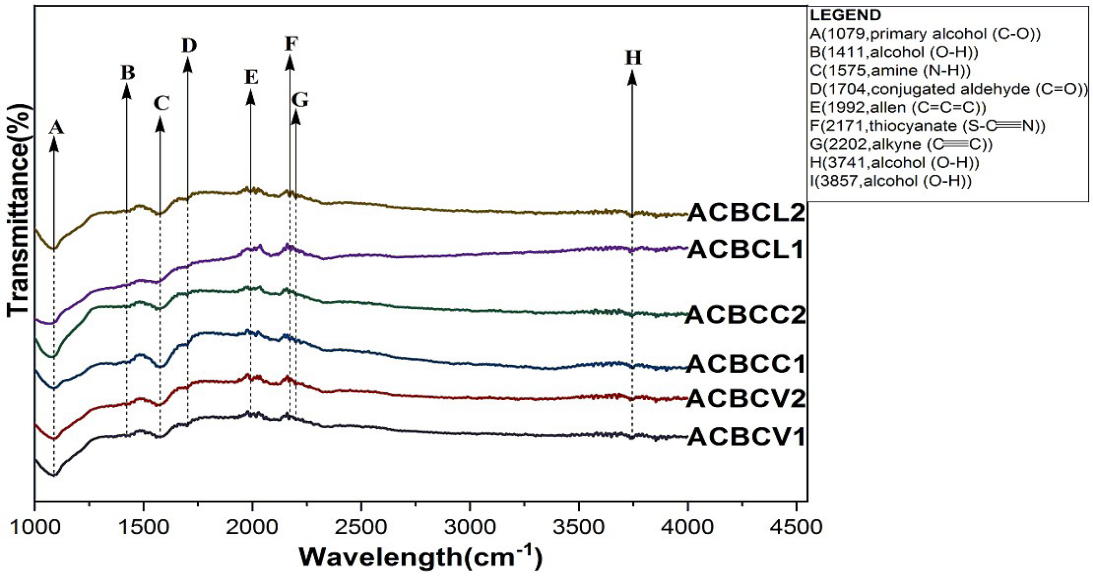

Figure S1. Surface functional group profile of activated phytoremediation and non-phytoremediation biochars.

ACBCV1: *Chrysopogon zizanioides* non-phytoremediation activated biochar, ACBCV2*:* activated *Chrysopogon zizanioides* phytoremediation biochar, ACBCC1*:* activates *Cymbopogon nardus* non-phytoremediation biochar, ACBCC2*:* activated *Cymbopogon nardus* phytoremediation biochar, ACBCL1: activated *Cymbopogon citratus* non-phytoremediation biochar, ACBCL2: activated *Cymbopogon citratus* phytoremediation biochar.

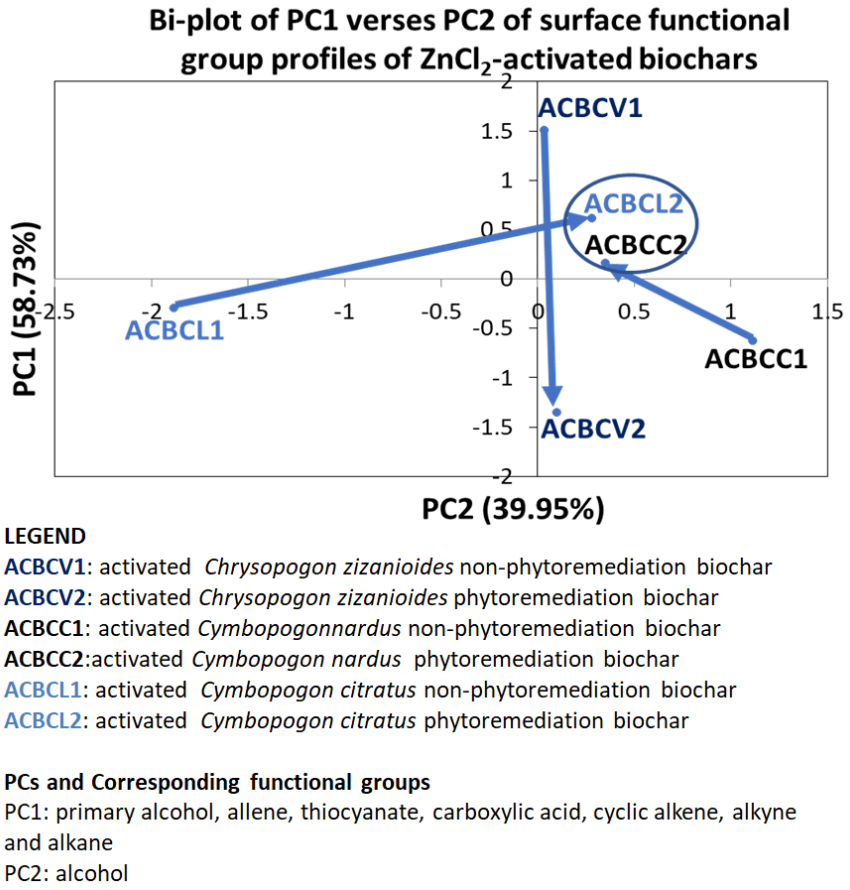

Figure S2. Biplot PC1 vs PC2 extracted from surface functional groups of Zn-Cl2-activated biochars from phytoremediation and non-phytoremediation biomasses.

ACBCV1: *Chrysopogon zizanioides* non-phytoremediation activated biochar, ACBCV2*:* activated *Chrysopogon zizanioides* phytoremediation biochar, ACBCC1*:* activated *Cymbopogon nardus* non-phytoremediation biochar, ACBCC2*:* activated *Cymbopogon nardus* phytoremediation biochar, ACBCL1: activated *Cymbopogon citratus* non-phytoremediation biochar, ACBCL2: activated *Cymbopogon citratus* phytoremediation biochar.

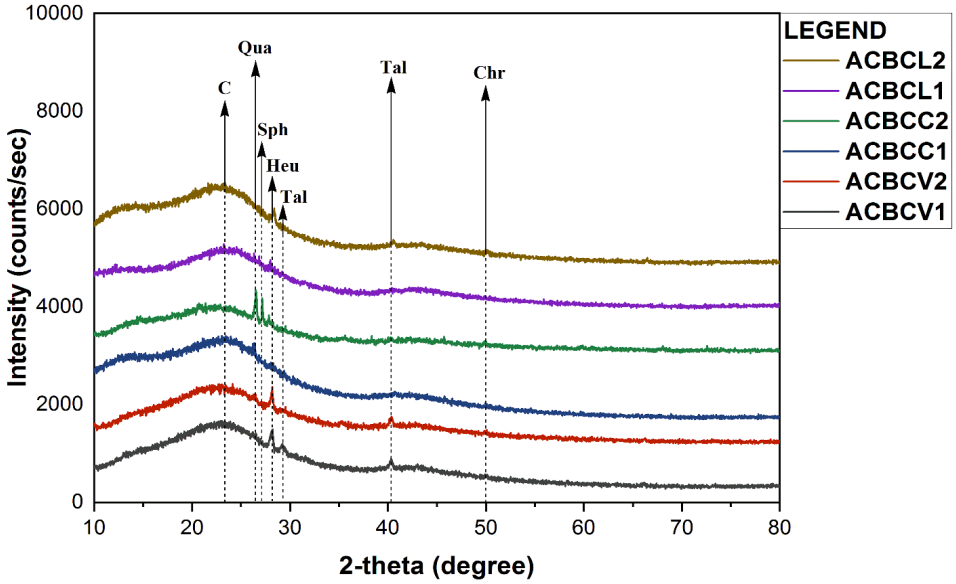

Figure S3. Minerals phases of $ZnCl_2$-activated biochars from non-phytoremediation and phytoremediation biomasses detected based on the x-ray diffraction analysis.

C: amorphous carbon, Qua: quartz, Sph: sphalerite, Heu: heulandite, Tal: talc, and Chr: chrysotile Biplot PC1 vs PC2 extracted from surface functional groups of Zn-Cl2-activated biochras from phytoremediation and non-phytoremediation biomasses.

ACBCV1: *Chrysopogon zizanioides* non-phytoremediation activated biochar, ACBCV2*:* activated *Chrysopogon zizanioides* phytoremediation biochar, ACBCC1*:* activated *Cymbopogon nardus* non-phytoremediation biochar, ACBCC2*:* activated *Cymbopogon nardus* phytoremediation biochar, ACBCL1: activated *Cymbopogon citratus* non-phytoremediation biochar, ACBCL2: activated *Cymbopogon citratus* phytoremediation biochar.

Table S1. Heavy metal contents of activated biochars derived from phytoremediation and non-phytoremediation biomasses

	Al	S	Cl	K	Ca	Cr	Mg	Fe	Ni	Cu	Zn	As	Rb
Sample	**ppm**												
ACBCL2	162.00	3840.00	7760.00	5395.00	6793.00	78.00	1075.00	8366.00	675.00	397.00	856.00	7.80	21.30
ACBCL1	58.00	2324.00	8830.00	9193.00	6054.00	21.00	234.00	786.00	ND	ND	158.00	ND	8.00
ACBCC2	71.00	2267.00	9870.00	6141.00	5687.00	67.00	587.00	7779.00	652.00	284.00	314.00	7.40	20.20
ACBCC1	54.00	910.00	10167.00	5340.00	5340.00	15.00	213.00	929.00	ND	ND	83.00	ND	5.10
ACBCV2	98.00	3982.00	9043.00	7670.00	5069.00	49.00	342.00	4084.00	612.00	198.00	217.00	5.50	34.40
ACBCV1	44.00	1031.00	10211.00	5232.00	4100.00	11.00	198.00	544.00	ND	ND	95.00	ND	10.50

Note: ACBCV1 is *Chrysopogon zizanioides* non-phytoremediation activated biochar, ACBCV2: *Chrysopogon zizanioides* phytoremediation activated biochar,
ACBCC1: *Cymbopogon nardus* non-phytoremediation activated biochar, ACBCC2: *Cymbopogon nardus* phytoremediation activated biochar,
ACBCL1: *Cymbopogon citratus* non-phytoremediation activated biochar, ACBCL2: *Cymbopogon citratus* phytoremediation activated biochar,
ppm: parts per million, and ND: not detected.

Table S2a. Regression coefficient (R^2) of adsorption isotherm plots

	PO_4^{3-} adsorption						
	R^2						
Sample name	**LG 1**	**LG 2**	**LG 3**	**LG 4**	**Freunlich**	**Temkin**	**Dubinin-Radushkevich**
BCV1	0.9813	0.9813	0.5239	0.5239	0.9264	0.9417	0.674
BCV2	0.8642	0.8642	0.0024	0.0024	0.8236	0.793	0.5719
BCC1	0.8228	0.08459	0.0034	0.0034	0.8251	0.9457	0.9568
BCC2	0.0742	0.0742	0.0147	0.0147	0.3081	0.3179	0.0805
BCL1	0.8979	0.8979	0.0438	0.0438	0.8996	0.9777	0.911
BCL2	0.9959	0.9959	0.7235	0.7235	0.9709	0.9231	0.6966
ACBCV1	0.9976	0.9976	0.7839	0.7839	0.9618	0.9378	0.7308
ACBCV2	0.9976	0.9976	0.7839	0.7839	0.9618	0.9378	0.7308
ACBCC1	0.8937	0.8937	0.0224	0.0224	0.8853	0.8362	0.916
ACBCC2	0.6672	0.6672	0.1237	0.1237	0.4431	0.4141	0.5252
ACBCL1	0.0007	0.0007	0.1297	0.1297	0.3689	0.7022	0.1754
ACBCL2	0.7821	0.7821	0.058	0.058	0.8744	0.8981	0.7513

Note: refers to LG Langmuir,
BCV1: *Chrysopogon zizanioides* non-phytoremediation biochar, BCV2: *Chrysopogon zizanioides* phytoremediation biochar,
BCC1: *Cymbopogon nardus* non-phytoremediation biochar,
BCL1: *Cymbopogon citratus*, non-phytoremediation biochar, BCL2: *Cymbopogon citratus* phytoremediation biochar,
ACBCV1: activated *Chrysopogon zizanioides* non-phytoremediation biochar, ACBCV2: activated *Chrysopogon zizanioides* phytoremediation biochar,
ACBCC1: activated *Cymbopogon nardus* non-phytoremediation biochar, ACBCC2: activated *Cymbopogon nardus* phytoremediation biochar,
ACBCL1: activated *Cymbopogon citratus* non-phytoremediation biochar, ACBCL2: activated *Cymbopogon citratus* phytoremediation

Table S2b. Regression coefficient (R^2) adsorption isotherm plots

	NO_3- adsorption						
	R^2						
Sample name	**LG 1**	**LG 2**	**LG 3**	**LG 4**	**Freunlich**	**Temkin**	**Dubinin-Radushkevich**
BCV1	0.9963	0.9963	0.0744	0.0744	0.9182	0.8508	0.7405
BCV2	0.6713	0.6713	0.1383	0.1383	0.8257	0.7938	0.6476
BCC1	0.7774	0.7774	0.0763	0.0763	0.7086	0.9433	0.9906
BCC2	0.8862	0.8862	4E-05	4E-05	0.8896	0.9713	0.9134
BCL1	0.0298	0.0298	0.0011	0.0011	0.2963	0.3328	0.0776
BCL2	0.9976	0.9976	0.5363	0.5363	0.9827	0.9131	0.7248
ACBCV1	0.9287	0.9287	0.1921	0.1921	0.9594	0.9922	0.7591
ACBCV2	0.9393	0.9393	0.2643	0.2643	0.9545	0.9867	0.7910
ACBCC1	0.9702	0.9702	0.0321	0.0321	0.8033	0.8170	0.9686
ACBCC2	0.6858	0.6858	0.0734	0.0734	0.4459	0.4212	0.5605
ACBCL1	0.8169	0.8169	0.1519	0.1519	0.7582	0.9205	0.9794
ACBCL2	0.8861	0.8861	0.3111	0.3111	0.8172	0.8886	0.9060

Note: LG refers to Langmuir, BCV1,
BCV1: *Chrysopogon zizanioides* non-phytoremediation biochar,
BCV2: *Chrysopogon zizanioides* phytoremediation biochar,
BCC1: *Cymbopogon nardus* non-phytoremediation biochar,
BCL1: *Cymbopogon citratus*, non-phytoremediation biochar,
BCL2: *Cymbopogon citratus* phytoremediation biochar,
ACBCV1: activated *Chrysopogon zizanioides* non-phytoremediation biochar,
ACBCV2: activated *Chrysopogon zizanioides* phytoremediation biochar,
ACBCC1: activated *Cymbopogon nardus* non-phytoremediation biochar,
ACBCC2: activated *Cymbopogon nardus* phytoremediation biochar,
ACBCL1: activated *Cymbopogon citratus* non-phytoremediation biochar,
ACBCL2: activated *Cymbopogon citratus* phytoremediation biochar.